Ethylene-Mediated Regulation of A2-Type CYCLINs Modulates Hyponastic Growth in Arabidopsis[1][OPEN]

Joanna K. Polko[2,3], Jop A. van Rooij[3], Steffen Vanneste, Ronald Pierik, Ankie M.H. Ammerlaan, Marleen H. Vergeer-van Eijk, Fionn McLoughlin[4], Kerstin Gühl[5], Gert Van Isterdael, Laurentius A.C.J. Voesenek, Frank F. Millenaar[6], Tom Beeckman, Anton J.M. Peeters[7], Athanasius F.M. Marée[8], and Martijn van Zanten[8,9]*

Plant Ecophysiology, Institute of Environmental Biology (J.K.P., R.P., A.M.H.A., M.H.V.-v.E., F.M., K.G., L.A.C.J.V., F.F.M., A.J.M.P., M.v.Z.), and Theoretical Biology and Bioinformatics (J.A.v.R.), Utrecht University, 3584 CH Utrecht, The Netherlands; Computational and Systems Biology, John Innes Centre, Norwich Research Park, Norwich NR4 7UH, United Kingdom (J.A.v.R., A.F.M.M.); Department of Plant Systems Biology, VIB, B–9052 Ghent, Belgium (S.V., G.V.I., T.B.); and Department of Plant Biotechnology and Bioinformatics, Ghent University, B–9052 Ghent, Belgium (S.V., G.V.I., T.B.)

Upward leaf movement (hyponastic growth) is frequently observed in response to changing environmental conditions and can be induced by the phytohormone ethylene. Hyponasty results from differential growth (i.e. enhanced cell elongation at the proximal abaxial side of the petiole relative to the adaxial side). Here, we characterize *Enhanced Hyponasty-D*, an activation-tagged Arabidopsis (*Arabidopsis thaliana*) line with exaggerated hyponasty. This phenotype is associated with overexpression of the mitotic cyclin *CYCLINA2;1* (*CYCA2;1*), which hints at a role for cell divisions in regulating hyponasty. Indeed, mathematical analysis suggested that the observed changes in abaxial cell elongation rates during ethylene treatment should result in a larger hyponastic amplitude than observed, unless a decrease in cell proliferation rate at the proximal abaxial side of the petiole relative to the adaxial side was implemented. Our model predicts that when this differential proliferation mechanism is disrupted by either ectopic overexpression or mutation of *CYCA2;1*, the hyponastic growth response becomes exaggerated. This is in accordance with experimental observations on *CYCA2;1* overexpression lines and *cyca2;1* knockouts. We therefore propose a bipartite mechanism controlling leaf movement: ethylene induces longitudinal cell expansion in the abaxial petiole epidermis to induce hyponasty and simultaneously affects its amplitude by controlling cell proliferation through CYCA2;1. Further corroborating the model, we found that ethylene treatment results in transcriptional down-regulation of *A2-type CYCLIN*s and propose that this, and possibly other regulatory mechanisms affecting CYCA2;1, may contribute to this attenuation of hyponastic growth.

Plants have acquired mechanisms to adjust growth and secure reproduction under unfavorable environmental conditions. Among the strategies to avoid adverse conditions is upward leaf movement, called hyponastic growth. This leaf reorientation is driven by unequal growth rates between adaxial and abaxial sides of the petiole (Cox et al., 2004; Polko et al., 2012b). Arabidopsis (*Arabidopsis thaliana*) exhibits hyponasty upon several environmental signals (e.g. submergence, waterlogging, proximity of neighboring vegetation, low red:far-red light ratios, reduced blue light fluence rates, low light intensities, and high temperatures; Millenaar et al., 2005, 2009; Mullen et al., 2006; Koini et al., 2009; Moreno et al., 2009; Van Zanten et al., 2009; Keuskamp et al., 2010; Keller et al., 2011; Vasseur et al., 2011; De Wit et al., 2012; Rauf et al., 2013; Dornbusch et al., 2014). Hyponasty alleviates the impact of environmental stresses (Van Zanten et al., 2010b). During submergence, it allows reestablishment of gas exchange with the atmosphere (e.g. Cox et al., 2003); at high plant densities, it positions the leaves in better lit layers of the canopy to improve light interception (e.g. De Wit et al., 2012); and at high temperatures, it improves the cooling capacity of the leaves (Crawford et al., 2012; Bridge et al., 2013). The cellular basis of hyponastic growth in *Rumex palustris* (Cox et al., 2004) and Arabidopsis (Polko et al., 2012b; Rauf et al., 2013) has been characterized. Ethylene causes reorientation of cortical microtubules (CMTs) in the petiole, which leads to longitudinal cell expansion in an approximately 2-mm-long epidermal cell zone at the proximal part of the abaxial side of the organ (Polko et al., 2012b).

The interactions between several hormones (e.g. ethylene, abscisic acid, GAs, and auxin) in controlling hyponasty under various conditions have been studied (Mullen et al., 2006; Benschop et al., 2007; Millenaar et al., 2009; Van Zanten et al., 2009, 2010b; Peña-Castro et al., 2011). The volatile phytohormone ethylene is a key component in the complex regulatory network of hyponastic growth. Ethylene is the trigger and a positive regulator of hyponastic growth in submerged and waterlogged Arabidopsis (Millenaar et al., 2005, 2009; Van Zanten et al., 2010b; Rauf et al., 2013) and a negative regulator of high temperature-induced hyponasty (Van Zanten et al., 2009), but is not involved in low light-induced hyponastic growth in this species (Millenaar et al., 2009). Abscisic acid antagonizes ethylene-induced hyponasty (Benschop et al., 2007) and is a positive

regulator of high temperature-induced hyponastic growth (Van Zanten et al., 2009). The growth-promoting GAs positively regulate hyponastic response to all three environmental signals (Peña-Castro et al., 2011), whereas auxins promote low light and high temperature-induced hyponastic growth (Millenaar et al., 2005; Koini et al., 2009; Van Zanten et al., 2009), as well as low red:far-red- and low blue light-induced hyponasty (Moreno et al., 2009; Keller et al., 2011). Finally, brassinosteroids also positively regulate ethylene-induced hyponasty (Polko et al., 2013).

Despite the extensive knowledge on hormonal regulation of hyponasty, little is known about the molecular genetic mechanisms that drive this response. One notable exception is the study by Rauf et al. (2013), who showed that hyponastic growth in Arabidopsis in response to root waterlogging is controlled by the NAC (for No Apical Meristem [NAM], Arabidopsis Transcription Activation Factor) transcription factor SPEEDY HYPONASTIC GROWTH that directly affects expression of the ethylene biosynthesis gene *1-AMINOCYCLOPROPANE-1-CARBOXYLIC ACID* (*ACC*) *OXIDASE5*.

Here, we followed a forward genetic approach to identify unique components that control hyponastic growth in Arabidopsis. From a population of activation-tagged plants (Weigel et al., 2000), we isolated *Enhanced Hyponasty-D* (*EHY-D*), which showed exaggerated hyponasty under exogenous ethylene application, low light intensities, and high temperature. We found that ectopic expression of the core cell cycle regulator *CYCLINA2;1* (*CYCA2;1*) caused the exaggerated ethylene-induced leaf movement of *EHY-D*. Mathematical analyses indicated that, besides promoting cell expansion, ethylene can also attenuate the amplitude of hyponasty by affecting differential cell proliferation in the petiole of wild-type plants. We suggest that this occurs through ethylene-dependent effects on CYCA2;1 levels, activity, or sensitivity in petioles of wild-type plants. The ethylene-mediated transcriptional regulation of *CYCA2;1* observed here could contribute to this. In *EHY-D*, however, ethylene-mediated effects on cell proliferation are overruled by ectopic *CYCA2;1* overexpression, which consequently results in enhanced hyponasty, in accordance with the predictions of our model. Correspondingly, *cyca2;1* knockout lines where ethylene cannot affect CYCA2;1-mediated cell proliferation also exhibited enhanced hyponasty. Our data therefore describe a mechanism by which hyponastic growth is kept within limits, through a bipartite role for ethylene: within the same organ, ethylene initiates hyponastic growth by promoting cell elongation, while simultaneously attenuating the response by regulation of A2-type CYCLIN-mediated cell proliferation.

RESULTS

Isolation and Cloning of *EHY-D*

To identify novel genetic components that control hyponastic growth, we conducted a forward genetic screen using a population of 35S activation-tagged Columbia (Col) plants (Weigel et al., 2000). A total of 17,500 plants were screened for their hyponastic response under 6 h of ethylene and low light treatment. The screen yielded 18 candidates with aberrant petiole angle (Polko et al., 2012a, 2013). Among the isolated lines was *EHY-D*, which showed an initial petiole angle similar to the wild type (20.5 ± 1.4 and 22.5 ± 1.4, respectively; Supplemental Table S1) and an exaggerated response to ethylene (Fig. 1, A and C) and low light (Fig. 1C). No other apparent visual differences were observed (Fig. 1B). The enhanced hyponasty phenotype was confirmed by quantitative analysis of leaf movement kinetics using a time-lapse digital camera setup (Fig. 1, D–F). In addition, high temperature also resulted in an enhanced response (Fig. 1, C and F), suggesting that a general genetic determinant of hyponastic growth is affected in *EHY-D*.

The phenotype cosegregated with the transgene in a 3:1 ratio (77.3 ± 2.0% glufosinate ammonium [Basta] resistant), indicating that *EHY-D* has a single T-DNA integration. Sequencing of the T-DNA flanking borders after thermal asymmetric interlaced-PCR (Liu et al., 1995) revealed that the insertion is on chromosome 5 in the intergenic region between *ETHYLENE RESPONSE FACTOR* (*ERF*)/*APETALA2* (*AP2*) transcription factor

[1] This work was supported by Utrecht University, the Research Foundation of Flanders (grant to S.V.), Netherlands Consortium for Systems Biology of the Netherlands Genomics Initiative/Netherlands Organization for Scientific Research (to J.A.v.R.), Biotechnology and Biological Sciences Research Council (grant no. BB/J004553/1 to A.F.M.M.), Interuniversity Attraction Poles (IAP VI/33 and IAP VII/29) of the Belgian Science Policy from the Belgian Federal Science Policy Office (to T.B.), and Netherlands Organization for Scientific Research VENI (grant no. 863.11.008 to M.v.Z.).

[2] Present address: Biology Department, University of North Carolina, 250 Bell Tower Dr., Genome Sciences Building, Chapel Hill, NC 27599.

[3] These authors contributed equally to the article.

[4] Present address: Department of Biochemistry and Molecular Biology, University of Massachusetts, 240 Thatcher Road, Amherst, MA 01003.

[5] Present address: Wageningen Seed Lab, Laboratory of Plant Physiology, Wageningen University, 6708 PB Wageningen Droevendaalsesteeg 4, The Netherlands.

[6] Present address: Nunhems Bayer CropScience, Napoleonsweg 152, 6083 AB Nunhem, The Netherlands.

[7] Present address: Institute of Education, Department of Biology, Utrecht University, Padualaan 8, 3584 CH Utrecht, The Netherlands.

[8] These authors contributed equally to the article.

[9] Present address: Molecular Plant Physiology, Institute of Environmental Biology, Utrecht University, Padualaan 8, 3584 CH Utrecht, The Netherlands.

* Address correspondence to m.vanzanten@uu.nl.

The author responsible for distribution of materials integral to the findings presented in this article in accordance with the policy described in the Instructions for Authors (www.plantphysiol.org) is: Martijn van Zanten (m.vanzanten@uu.nl).

J.K.P., S.V., A.M.H.A., M.H.V.-v.E., F.M., K.G., G.V.I., and M.v.Z. performed the experiments; J.A.v.R. and A.F.M.M. performed the mathematical and in silico modeling; R.P., L.A.C.J.V., F.F.M., T.B., A.J.M.P., A.F.M.M., and M.v.Z. supervised the experiments; J.K.P., J.A.v.R., S.V., R.P., A.J.M.P., A.F.M.M., and M.v.Z. wrote the article, with contributions of all the authors.

[OPEN] Articles can be viewed without a subscription.

www.plantphysiol.org/cgi/doi/10.1104/pp.15.00343

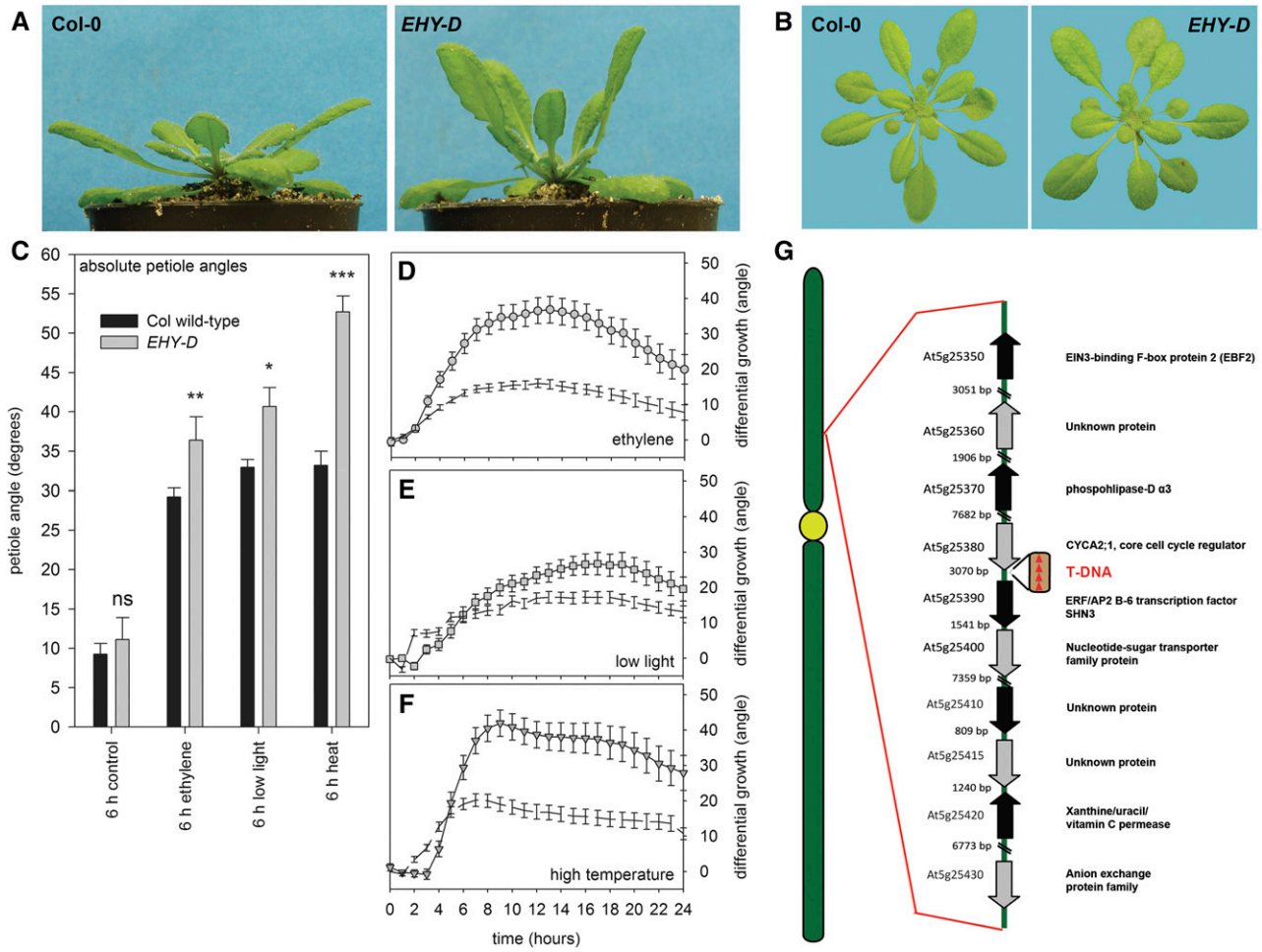

Figure 1. Hyponastic response and cloning of *EHY-D*. A, Leaf angle phenotype of the wild type and *EHY-D* after 10-h ethylene treatment. B, *EHY-D* and the wild-type rosette phenotype. C, Absolute petiole angles of *EHY-D* (gray bars) and the wild type (black bars) after 6-h control conditions, ethylene (1.5 μL L^{-1}), low light (20 μmol m^{-2} s^{-1}), and high temperature (38°C) treatment. Significance levels (2-tailed Student's *t* test; ns, not significant): *,$P < 0.05$; **,$P < 0.01$; and ***, $P < 0.001$. D–F, Hyponastic growth kinetics of *EHY-D* (gray symbols) compared with the wild type (dashed lines) upon treatment with ethylene (circles; D), low light (squares; E), and high temperature (triangles; F). Angles in D to F resulted from pairwise subtraction (Benschop et al., 2007). Error bars are SEM; $n > 10$. G, Representation of the *EHY-D* transfer DNA (T-DNA) insertion site (box) on chromosome 5. Red arrowheads indicate the direction of the 35S transcriptional enhancers. Genes in the vicinity, their Arabidopsis Genome Initiative codes, and annotation are depicted as arrows, pointing in the direction of transcription. Physical distances between the genetic elements are in base pairs.

subfamily B-6; *SHINE3* (*SHN3*; At5g25390; Nakano et al., 2006) and the mitotic checkpoint regulator *CYCA2;1* (At5g25380; Fig. 1G).

Genes causal for observed phenotypes are often flanking or in the direct vicinity of the T-DNA insertion site (Weigel et al., 2000). Therefore, we quantified the relative transcript levels of the genes within a 15-kb region up- and downstream of the T-DNA integration site by quantitative reverse transcription (qRT)-PCR under control conditions and after application of ethylene. Some of the tested genes were mildly up-regulated after 3 h of ethylene treatment compared with control conditions in wild-type Col (Table I). This included *ETHYLENE INSENSITIVE3* (*EIN3*)-*BINDING F-BOX PROTEIN2* that was previously shown to be ethylene inducible (Potuschak et al., 2003). In *EHY-D*, only the two genes directly flanking the T-DNA insertion border (*SHN3* and *CYCA2;1*) were overexpressed compared with wild-type Col, and this was true under both control and ethylene conditions (Table I). This suggests that one of these genes is causal for the exaggerated hyponastic growth phenotype of *EHY-D*.

Overexpression of *CYCA2;1* Mimics the *EHY-D* Hyponastic Growth Phenotype

SHN3 encodes a member of the *ERF* family. ERFs control many developmental and physiological processes, including several ethylene-mediated responses (Nakano et al., 2006). Using overexpression lines in the Wassilewskija (Aharoni et al., 2004) and Col backgrounds (isolated

Table I. *Relative expression levels (± SEM) of genes flanking the EHY-D T-DNA insertion, compared with the wild-type Col, in control (air; 3 h) and ethylene-enriched conditions (3 h; see also Fig. 1G)*

Arabidopsis Genome Initiative code	Gene Ontology (GO Annotation)	Relative Expression ± SEM			
		Control		Ethylene	
		Col	*EHY-D*	Col	*EHY-D*
At5g25430	HCO_3-anion-exchange protein family protein	1.00 ± 0.16	1.17 ± 0.15	1.15 ± 0.18	0.84 ± 0.10
At5g25420	Xanthine/uracil/vitamin C permease	1.00 ± 0.30	0.77 ± 0.62	0.62 ± 0.48	1.13 ± 0.39
At5g25415	Unknown protein	1.00 ± 0.60	1.91 ± 1.40	2.84 ± 1.58	0.50 ± 0.26
At5g25410	Unknown protein	1.00 ± 0.31	0.65 ± 0.26	2.56 ± 1.47	0.90 ± 0.69
At5g25400	Nucleotide-sugar transporter family protein	1.00 ± 0.19	1.22 ± 0.26	1.48 ± 0.49	1.01 ± 0.14
At5g25390	ERF/AP2 B-6 transcription factor, SHN3	1.00 ± 0.28	3.18 ± 0.95	1.11 ± 0.53	3.24 ± 0.43
At5g25380	CYCA2;1, core cell cycle regulator	1.00 ± 0.30	142.45 ± 21.71	0.89 ± 0.30	106.58 ± 13.61
At5g25370	Phospohlipase-D α3	1.00 ± 0.15	1.13 ± 0.13	1.13 ± 0.23	1.19 ± 0.24
At5g25360	Unknown protein	1.00 ± 0.06	2.24 ± 0.48	2.23 ± 0.21	1.12 ± 0.08
At5g25350	EIN3-binding F-box protein2	1.00 ± 0.12	2.27 ± 0.61	2.92 ± 0.96	0.66 ± 0.19

from the collection described in Weiste et al., 2007), we tested if *SHN3* overexpression could be responsible for the observed exaggerated hyponasty in *EHY-D*. However, overexpression of *SHN3* did not result in enhanced hyponastic responses in either the Col or Wassilewskija background (Supplemental Fig. S1). This indicates that *SHN3* overexpression in *EHY-D* is not causing its exaggerated hyponastic growth phenotype.

CYCA2;1, the highly up-regulated gene directly flanking the *EHY-D* locus (Fig. 1G), belongs to a small gene family of G2-to-M cell cycle regulators (Yoshizumi et al., 2006; Vanneste et al., 2011). To test if *CYCA2;1* overexpression could explain the *EHY-D* phenotype, we generated *35S*::*CYCA2;1* plants. As observed in *EHY-D*, hyponastic growth was enhanced in four independent *CYCA2;1* overexpression lines (Fig. 2, A–C; Supplemental Figs. S2 and S3). The differences in hyponastic growth response between the independent lines was positively correlated with the respective *CYCA2;1* expression levels (Supplemental Fig. S3). Moreover, a mutant defective in the conserved and specific *A2-type CYCLIN* repressor *INCREASED LEVEL OF POLYPLOIDY1-2* (*ilp1-2*), which results in enhanced expression of all *A2-type CYCLIN* family members (Yoshizumi et al., 2006), also showed exaggerated hyponastic growth under ethylene exposure (Fig. 2D). This response was comparable with *EHY-D* and *35S*::*CYCA2;1* lines. Consistently, the *ILP1-D* activation-tagged line with decreased expression of all four *A2-type CYCLIN*s (Yoshizumi et al., 2006) showed reduced hyponastic growth (Fig. 2E).

Transcription of other *A2-type CYCLIN* family members (Vandepoele et al., 2002) and several other cell cycle marker genes (Yoshizumi et al., 2006) was not distinctly affected in whole petioles of *EHY-D* (Fig. 2F) in either control or ethylene conditions. Taken together, these data demonstrate that overexpression of *CYCA2;1* is sufficient to explain the *EHY-D* hyponastic growth phenotype.

Surprisingly, when we assayed the requirement of functional *CYCA2;1* for hyponastic growth, we found that two independent knockout alleles of *cyca2;1* also showed an exaggerated response to ethylene, low light, and high temperature treatment (Fig. 2, G and H; Supplemental Fig. S4; Supplemental Table S1). Because it has been reported that reduced *CYCA2;2* expression in *erecta* loss-of-function mutants can be compensated for by ectopic up-regulation of *CYCA2;3* (Pillitteri et al., 2007), we tested for compensatory up-regulation of other *A2-type CYCLIN*s in *cyca2;1* mutant petioles by qRT-PCR. However, our qRT-PCR experiments did not reveal ectopic up-regulation of *CYCA2;2*, *CYCA2;3*, or *CYC2A2;4* in petiole tissues of the *cyca2;1-2* mutant (Supplemental Fig. S4). Similar to *EHY-D* (Fig. 2F), these genes were also not affected in the *35S*::*CYCA2;1* line (Supplemental Fig. S4). Therefore, compensatory transcriptional up-regulation of other *A2-type CYCLIN*s in the petiole probably cannot explain the enhanced hyponastic growth response of *cyca2;1* mutants. However, from these data, we cannot exclude that changes in spatiotemporal expression of other *A2-type CYCLIN*s affect the hyponastic growth response.

Therefore, we also analyzed *cyca2;2-1*, *cyca2;3-1*, and *cyca2;4-1* insertional mutants (Vanneste et al., 2011). In contrast to the *cyca2;1* mutants (Fig. 2, G and H), these single mutants did not show an altered hyponastic growth phenotype in response to ethylene (Supplemental Fig. S5). However, when combined with other mutations in the *A2-type CYCLIN* family, the exaggerated *cyca2;1* hyponastic growth was lost and was in some cases even lower than the wild type (Supplemental Fig. S5), suggesting that misregulation of other *CYCA2*s could be related to the *cyca2;1* mutant phenotype. This is consistent with the results of *ILP1-D* where all *A2-type CYCLIN*s were transcriptionally down-regulated (Fig. 2E) and demonstrates involvement of other A2-type CYCLINs in the control of hyponastic growth. To address this, we analyzed the hyponastic growth of a *CYCA2;2* overexpression line. Similar to the *EHY-D* and *35S*::*CYCA2;1* lines, the *35S*::*CYCA2;2* line also showed enhanced hyponasty in response to ethylene and low light, but not in response to high temperature (Supplemental Fig. S5). In addition, the initiation of the response to low light and high temperatures was delayed, suggesting that, besides CYCA2;1, other A2-type CYCLINs are also biochemically competent in modifying hyponastic growth responses.

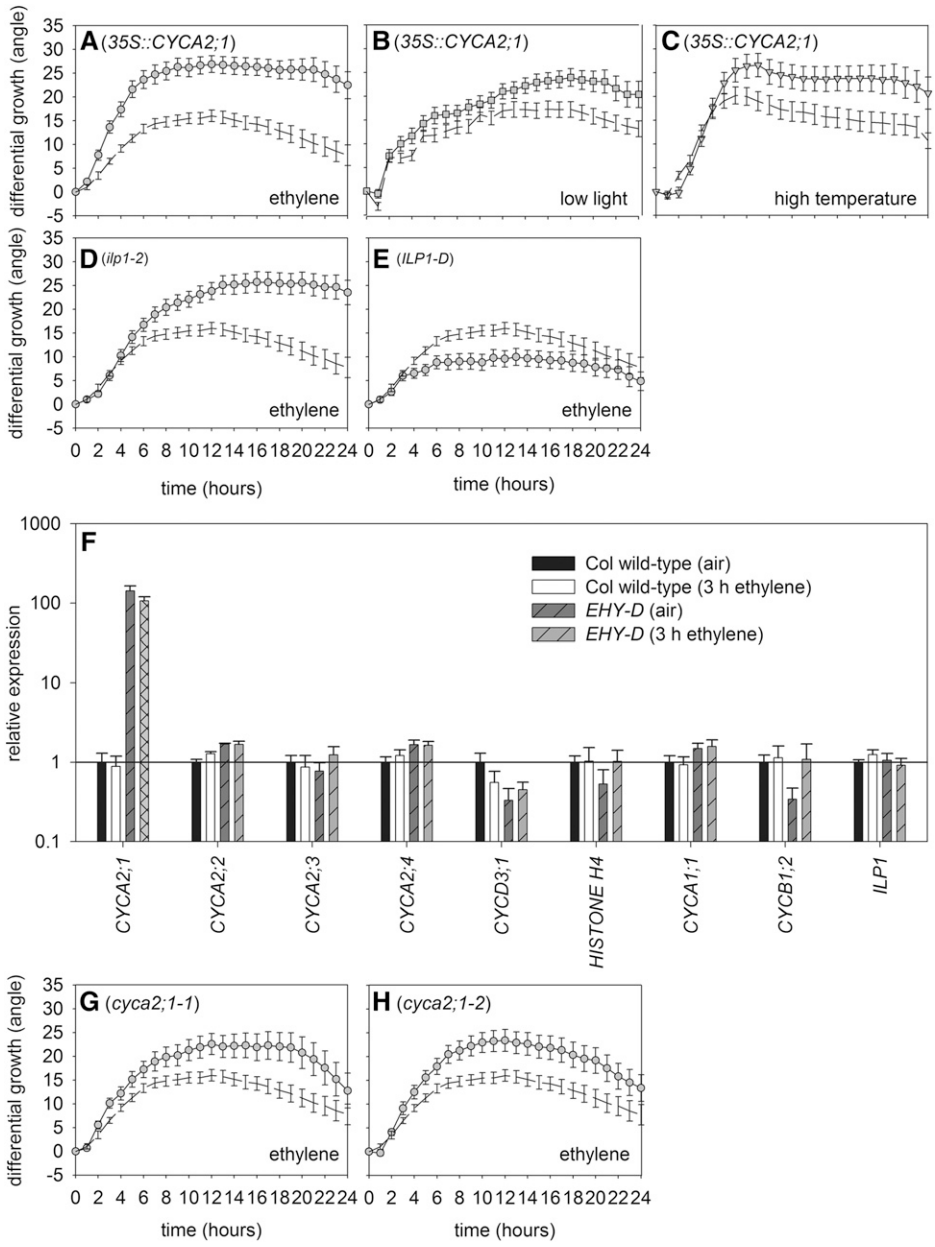

Figure 2. Ectopic *CYCA2;1* overexpression and *cyca2;1* knockout lead to exaggerated hyponastic growth amplitude. A to E, Hyponastic growth kinetics of plants misexpressing *CYCA2;1* (symbols) compared with the wild type (dashed lines). A to C, *35S*::*CYCA2;1* upon ethylene (circles; A), low light (squares; B), and high temperature (triangles; C) treatment. D, *ilp1-2* null allele (circles) upon ethylene treatment. E, *ILP1-D* enhancer-tagged line (circles) upon ethylene treatment. F, Expression of *A2-type CYCLIN*s and cell cycle marker genes: *CYCD3;1*, *HISTONE H4*, *CYCA1;1*, *CYCB1;2* (G1-, S-, G2-, and M-phase-specific, respectively; Yoshizumi et al., 2006), and *ILP1*, in whole petioles of Col wild type (black and white bars) and *EHY-D* (gray, dashed bars) in control conditions (black and dark-gray) and after 3-h ethylene treatment (white and light-gray). Expression values were normalized to 1 for the wild-type control. Error bars are SEM, $n \geq 4$. G and H, Hyponastic growth kinetics of *cyca2;1-1* (G) and *cyca2;1-2* (H) knockout mutants (symbols) compared with the wild type (dashed lines). Error bars are SEM; $n \geq 10$. For details, see Figure 1.

Ethylene Suppresses Expression of Mitotic Genes in the Petiole

To determine if CYCA2;1 is specifically involved in hyponasty or modifies a general component in ethylene-mediated growth responses, we assayed ethylene-dependent inhibition of hypocotyl elongation in dark-grown seedlings (Guzman and Ecker, 1990). No differences in elongation were detected in *EHY-D*, *35S*::*CYCA2;1*, and *cyca2;1-2* compared with the wild type (Fig. 3A) in the presence of increasing concentrations of the ethylene biosynthetic precursor ACC. This indicates that *CYCA2;1* levels do not affect ethylene sensitivity of the hypocotyls. Additionally, ethylene release from vegetative rosettes of these lines was similar to that of the wild type (0.65 ± 0.13 in *EHY-D*, 0.64 ± 0.09 in *35S*::*CYCA2;1*, and 0.52 ± 0.06 in *cyca2;1-2* compared with 0.65 ± 0.13 nL g FW^{-1} h^{-1} in the wild type). These results suggest that *CYCA2;1* regulation does not modify general ethylene-mediated growth responses, but may have a specific role in hyponastic growth.

To evaluate if ethylene affects *A2-type CYCLIN* expression in the petioles, we first assayed promoter activity of the four *A2-type CYCLIN*s by promoter::GUS analyses (Burssens et al., 2000; Vanneste et al., 2011). All *A2-type CYCLIN* promoters were active in meristematic tissues at the rosette center and were mainly, but not exclusively, localized in vascular tissues (Supplemental Fig. S6). Observations of radial sections of whole petioles (Supplemental Fig. S7), detailed analysis of proximal and distal petiole tissues (relative to the meristem;

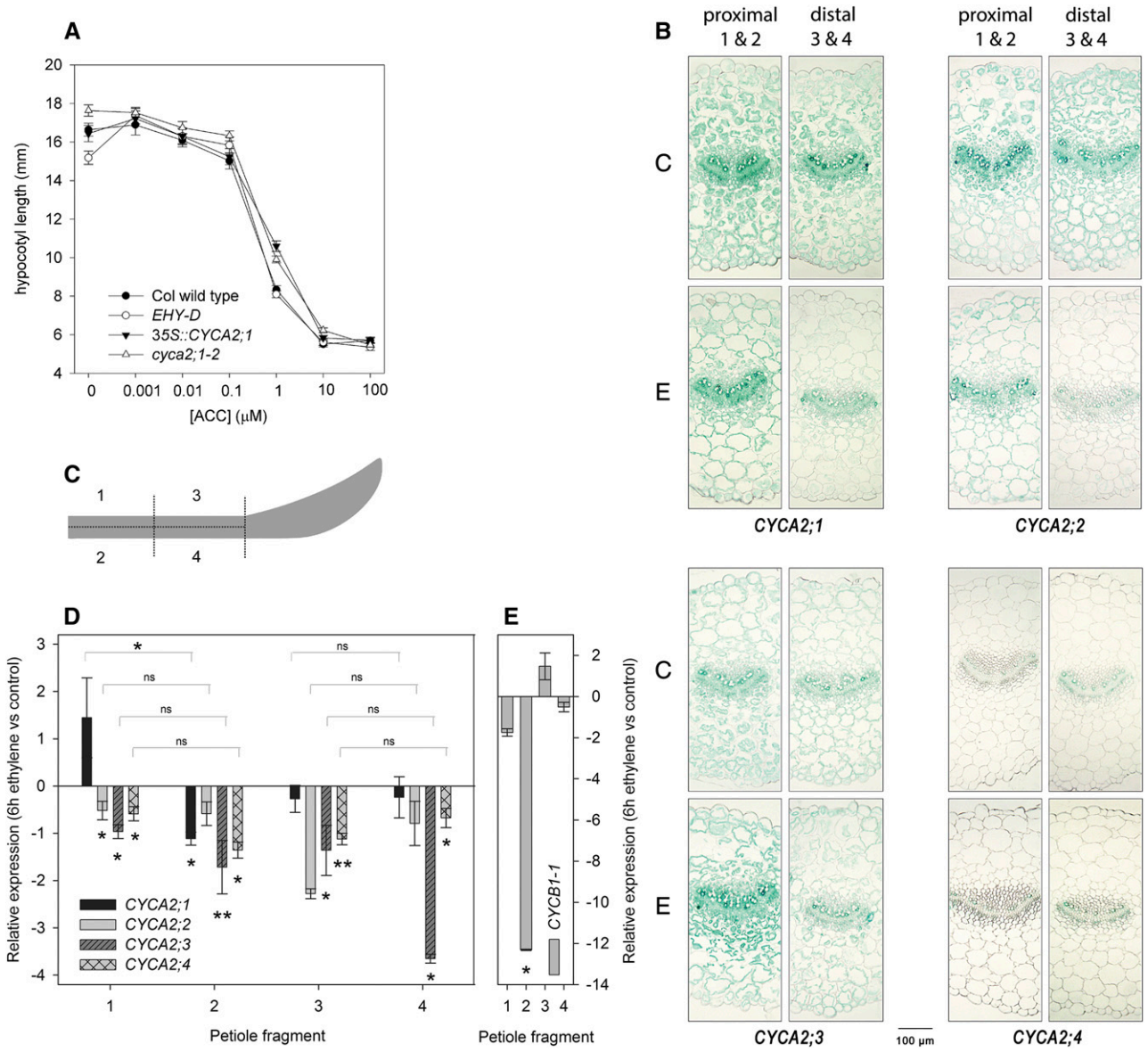

Figure 3. Ethylene sensitivity of *CYCA2;1* misexpressing lines and ethylene effects on *CYCLIN* transcription. A, Hypocotyl elongation assay of etiolated seedlings grown in the presence of the ethylene precursor ACC. *EHY-D* (white circles), *35S::CYCA2;1* (black triangles), *cyca2;1-2* (white triangles), and wild type (black circles). Error bars are the SD; $n \geq 22$. B, Histochemical analysis of ethylene effects on *A2-type CYCLIN* promoter activity of plants carrying individual *A2-CYCLIN* family promoters fused to the *GUS* reporter gene. Transverse sections (200 μm thick) of corresponding fragments (1–4, as shown in C) treated with ethylene (E; 1.5 μL L^{-1}) for 6 h, or kept in control (C; air) conditions. C, Representation of petiole quarters used for transcription analysis of *A2-type CYCLIN*s (D) and *CYCB1;1* (E) upon 6-h ethylene exposure in wild-type plants. Data are mean relative expression values; error bars are SEM, $n \geq 4$. Significance levels under the bars reflect the difference between expression in air control and after ethylene treatment in the respective petiole quarter, and significance levels above the gray brackets represent the difference between the adaxial and abaxial side of the petiole fragments represented in C; ns, nonsignificant; *, $P < 0.05$; and **, $P < 0.01$.

Supplemental Fig. S7), and transverse sections (Fig. 3B) of histochemically stained petioles were variable but showed overall that ethylene results in transcriptional repression of *A2-type CYCLIN*s after 6 h of ethylene treatment, despite the fact that the GUS protein is relatively stable and transcriptional down-regulation was not yet measurable after 3 h by qRT-PCR (Fig. 2F). These results suggest that ethylene suppresses *A2-type CYCLIN* expression in Arabidopsis petioles.

To corroborate these findings based on promoter::GUS analysis, we analyzed *A2-type CYCLIN* expression in microdissected fragments of wild-type petioles (Fig. 3C) by qRT-PCR. This revealed that *CYCA2;2*, *CYCA2;3*, and *CYCA2;4* are transcriptionally down-regulated

after prolonged (6 h) ethylene treatment in all four fragments (Fig. 3D). Notably, *CYCA2;1* was also generally down-regulated, including in the proximal-abaxial section (fragment 1, Fig. 3, C and D), but appeared modestly up-regulated at the proximal-adaxial side (Fig. 3D).

Because A2-type CYCLINs control a cell cycle checkpoint upstream of the expression of mitotic regulators such as B-type CYCLINs (Vanneste et al., 2011), we anticipated and confirmed that ethylene also represses expression of the mitotic CYCLIN, *CYCB1;1*, in these tissues (Fig. 3E). These results are consistent with a suppression of proliferation by ethylene in petiole tissues.

Endoreduplication Cannot Explain Exaggerated Hyponastic Growth in *EHY-D* and *35S::CYCA2;1*

A2-type CYCLINs have been implicated in the control of local cell cycle progression to fine tune development (Vanneste et al., 2011). More specifically, their expression levels can affect the local balance between cell proliferation and endoreduplication, a process of consecutive rounds of DNA replication without mitosis (Yu et al., 2003; Imai et al., 2006; Yoshizumi et al., 2006) that has been associated with cells that have an increased capacity for elongation (Cheniclet et al., 2005; Roeder et al., 2010). Despite previous reports on ethylene-related changes in endoreduplication in hypocotyls (Gendreau et al., 1999; Dan et al., 2003), we did not find significant ethylene-dependent differences in ploidy levels in microdissected proximal and distal fragments of wild-type petioles (Supplemental Fig. S8). However, we did observe slightly different ploidy levels between distal and proximal regions of the petiole (Supplemental Fig. S8), as well as small but significant differences in the 2n, 4n, 16n, and 32n classes between the wild type and *EHY-D* ($P = 0.041$, $P = 0.036$, $P = 0.007$, and $P = 0.05$, respectively; Supplemental Fig. S8). However, no significant differences were detected between the wild type and *35S::CYCA2;1* (except for the 4n class, $P = 0.025$; Supplemental Fig. S8), making it unlikely that the exaggerated hyponastic growth of both *CYCA2;1*-overexpressing lines (*EHY-D* and *35S::CYCA2;1*) can be explained by changes in ploidy levels. Moreover, a dominant negative *CYCLIN-DEPENDENT KINASE B1-1* (*CDKB1;1*)-overexpressing line with enhanced ploidy levels in aerial organs (Boudolf et al., 2009) showed ethylene-induced hyponastic growth that was indistinguishable from the wild type (Supplemental Fig. S8). Together, these data argue against a major role of endoreduplication in the exaggerated hyponastic growth in *EHY-D*.

Ectopic Overexpression of *CYCA2;1* Comprises Ethylene-Mediated Differential Cell Proliferation during Hyponastic Growth

We examined if enhanced hyponasty in *35S::CYCA2;1* is due to enhanced cell expansion in the petiole compared with the wild type. Measurements of epidermal cell lengths revealed that significant cell expansion in *35S::CYCA2;1* under ethylene treatment occurs in an approximately 2-mm epidermal zone at the proximal abaxial side of the petiole (Fig. 4, A and B). The pattern of changes in cell size strongly resembles the pattern previously observed in wild-type Arabidopsis Col plants (Fig. 4, C and D; Polko et al., 2012b; Rauf et al., 2013). Moreover, *35S::CYCA2;1* showed a similar ethylene-induced CMT reorientation as described previously for wild-type plants (Polko et al., 2012b; Supplemental Fig. S9). Although this suggests that the exaggerated hyponastic growth in *35S::CYCA2;1* is not due to differences in cell expansion compared with the wild type, this cannot be concluded without taking cell proliferation into account (see Supplemental Text S1). However, due to experimental constraints, cell division rates cannot be derived from empirical in vivo cell length measurements (see Supplemental Text S1). This is because both time lapse imaging of cell division as well as destructive measurements directly interfere with the hyponastic response itself. Nevertheless, the dynamic petiole shape and static cell size distributions as observed from epidermal imprints (Fig. 4, A–D) together provided sufficient information to allow for a mathematical analysis that indirectly estimates the contribution of cell divisions within the petiole. Using such a mathematical approach, we calculated relative division rates between abaxial versus adaxial cells, which is sufficient to describe the role of cell division in petiole hyponasty. Theoretical details can be found in the "Materials and Methods" and Supplemental Texts S2 and S3. The mathematical analysis showed that, in wild-type plants, ethylene treatment strongly increased the bias toward adaxial cell proliferation in the proximal region of the petiole, with adaxial cell division rates during ethylene treatment being up to 80% higher than abaxial cell division rates (Fig. 4, E and F). This indicates that, in this region, ethylene triggers either increased adaxial cell proliferation or decreased abaxial cell proliferation. Our qRT-PCR and GUS analysis showed that ethylene in general suppresses cell proliferation markers (Fig. 3, B and D; Supplemental Figs. S6 and S7). The most likely scenario would therefore be a decrease in cell proliferation. The analysis predicts that a local reduction of cell proliferation rate in an approximately 2-mm-long epidermal cell zone at the proximal part of the abaxial side of the petiole is required to match the measured amplitude of hyponastic growth in the wild type. This is in accordance with Polko et al. (2012b), where a comparable analysis showed that, under the assumption that abaxial and adaxial cell proliferation rates are equal, the observed changes in abaxial cell elongation rates during ethylene treatment result in a larger hyponastic response in comparison with what was experimentally observed. We observed that the *35S::CYCA2;1* line was lacking such increased bias toward adaxial cell proliferation after ethylene treatment. Instead, in this line, the cell proliferation profile in ethylene was estimated to be highly similar to the cell proliferation profile in the untreated controls (Fig. 4, E and F). In other

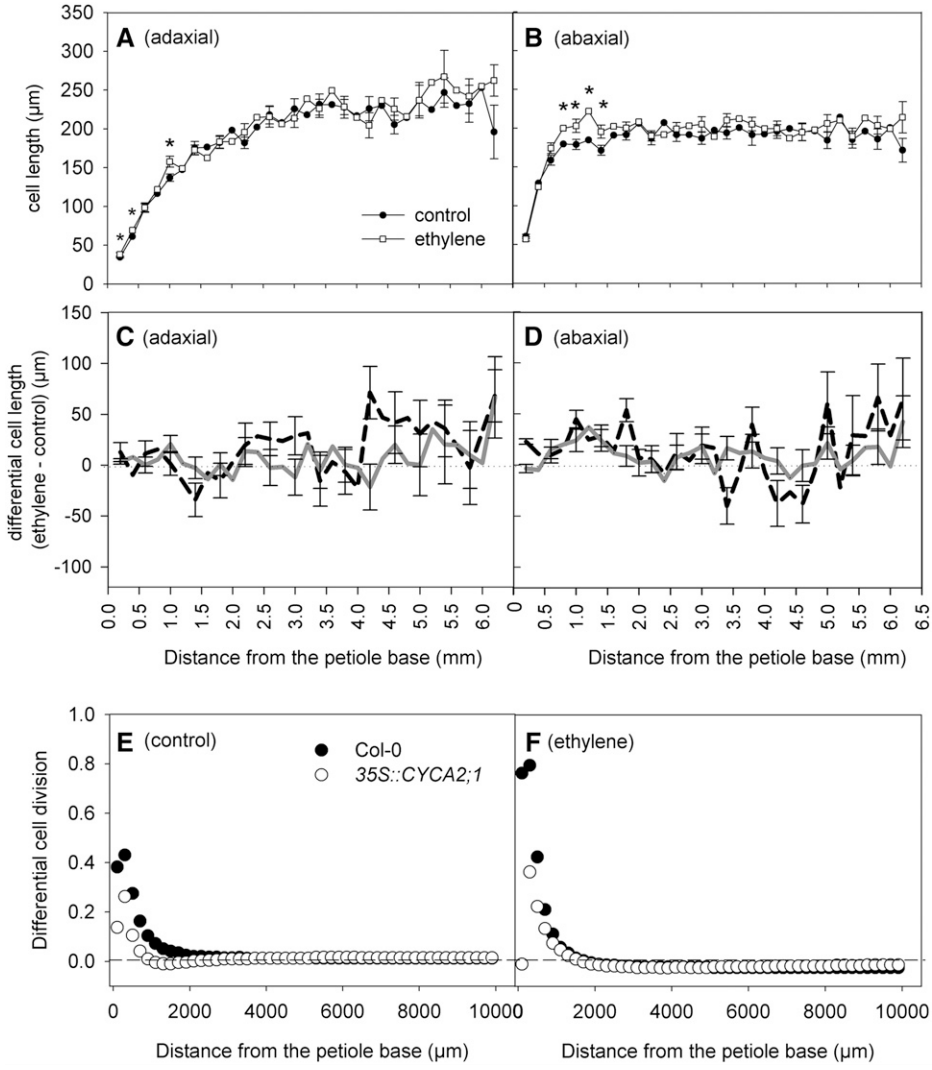

Figure 4. Ethylene effect on CYCA2;1-mediated cell expansion and proliferation. A and B, Average epidermal cell lengths as experimentally measured from *35S::CYCA2;1* petioles per 200-μm class, according to their distance relative to the proximal side of the petiole of adaxial (A) and abaxial (B) epidermal cells after 10-h control (black circles) and 10-h ethylene (white squares) treatment. Significance levels (2-tailed Student's *t* test): $*P < 0.05$, n = 13–15. C and D, Differential experimentally determined cell growth after 10-h ethylene treatment over the length classes in *35S::CYCA2;1* (gray lines; this study) in comparison with the wild type (black dashed line as has been published in Polko et al., 2012b; Fig. 2). Error bars are SEM. E and F, Calculated relative cell proliferation after 10-h control (E) and ethylene treatment (F) in the wild type (black circles) and *35S::CYCA2;1* (white circles), presented as the difference (ratio) between adaxial and abaxial cell proliferation rate. Values greater than 0 indicate that adaxial proliferation is predominant, and 0 means equal cell proliferation on both sides.

words, cell proliferation rates in *35S::CYCA2;1* are predicted to be comparable between control and ethylene treatment, whereas in the wild type, ethylene exposure represses abaxial cell divisions relative to adaxial cell divisions.

Together, this suggests that ethylene controls differential cell proliferation in the petiole, thereby affecting the amplitude of ethylene-induced hyponastic growth. Our calculations indicate that ethylene causes enhanced abaxial cell elongation leading to hyponastic growth, while at the same time suppressing proliferation, thus attenuating hyponasty. In *35S::CYCA2;1*, this secondary control mechanism is overruled, leading to exaggerated hyponastic growth.

In Silico Modeling of Hyponastic Growth Corroborates that Absence of Differential Cell Proliferation Leads to Exaggerated Hyponasty

Tissue growth can be described by the combination of cell expansion and cell division. However, cell divisions, as opposed to cell elongation, do not immediately generate volumetric tissue growth (only extra cells). Therefore, divisions can only have an indirect effect on tissue growth (Harashima and Schnittger, 2010). The effect of cell division on tissue growth depends on the specific relationship between cell size and cell expansion, as is discussed in Supplemental Text S4. Our mathematical analysis on petiole epidermal cell lengths indicated that the amplitude of ethylene-induced hyponastic growth is mediated by a differential regulation of cell division, and that the enhanced hyponastic growth response in *35S::CYCA2;1* is correlated with an absence of reduction in cell division (Fig. 4, E and F), suggesting that CYCA2;1 has a role in the mechanism that mediates the hyponastic growth response specifically via reduced abaxial cell proliferation. To further explore the relationship between (abaxial) cell division and the hyponastic growth response, we developed an in silico model of the Arabidopsis petiole. With the model, we simulated ethylene-induced hyponastic growth for different scenarios of cell expansion: linear, exponential, logistic,

and logarithmic growth and division rates. Since it has been shown that the epidermal cell layer is sufficient to drive and restrict plant growth (Savaldi-Goldstein et al., 2007), we modeled only the epidermal layers of the abaxial and adaxial sides of the petiole (Fig. 5A). The experimental data showed that cell size increases along the petiole (Fig. 4, A and B). We simplified the growth and cell cycle dynamics by assuming in the first instance that, apart from the adaxial-abaxial differences, the petiole is spatially homogenous (i.e. that cell expansion and division are not influenced by their proximal-distal position in the petiole; for details on the in silico modeling, see "Materials and Methods" and Supplemental Text S5).

Because the precise relationship between cell size and cell expansion dynamics is not well established (see Supplemental Text S5), we simulated hyponastic growth of the petiole for different possible scenarios of cell expansion, namely linear, exponential, logistic, and logarithmic, and combined this with different cell division scenarios.

A first round of simulations assessed the possible effect of reduced cell division in the proximal abaxial region on petiole shape for the different possible cell expansion scenarios, other than an increase in abaxial cell expansion due to ethylene treatment, and analyzed whether a reduction in cell proliferation (ranging from 0%–100%) within that region could indeed attenuate the hyponastic response that would be expected without reduction in abaxial cell proliferation (Fig. 5B). These simulations support the idea that reduction in abaxial cell proliferation leads to reduction in hyponastic petiole curvature, except when cell expansion is exponential. As explained in Supplemental Text S4, however, exponential cell expansion implies that the occurrence of cell divisions has no influence whatsoever on the tissue growth, which is an unrealistic scenario. These simulations thus indicate that a decrease in abaxial cell division is expected to reduce hyponastic growth.

Next, we explored the role of cell expansion arrest during cell division. In the simulations described earlier, we did not take into account that the cell division event itself could directly affect the cell expansion. It is very likely, however, that cell expansion is arrested for a certain amount of time when the cell goes through mitosis (Beemster and Baskin, 1998; Grieneisen et al., 2007). Figure 5C shows that prolonged periods of arrest in expansion during mitosis can counterbalance the effect of reduced abaxial cell division on petiole curvature, but only for a duration of the expansion arrest that is unrealistically long.

Next, we used this model to evaluate the impact of misregulated cell proliferation, as expected for overexpression or mutation of *CYCA2;1* (Fig. 5, D–G). To capture the complete petiole shape, we used the observation that cell division and elongation are limited to the proximal 3 mm of the petiole (Fig. 4, A and B). The shape of the distal part of the petiole is therefore considered conserved over the period of the experiment (see Supplemental Text S5). For all three genetic backgrounds (wild type, *35S*::*CYCA2;1*, and *cyca2;1*), we parameterized that ethylene treatment increases abaxial cell elongation (Fig. 4, A and B), and that mitosis causes a 1-h arrest in cell expansion. Following our hypothesis and the simulations described earlier, we assumed that, in the wild type, abaxial cell division decreases during ethylene-induced hyponastic growth (Fig. 5E). Alternatively, we modeled genetic backgrounds that lack such differences between abaxial and adaxial cell division by setting overall cell division rates to be constitutively higher and constitutively lower, reflecting scenarios of overexpression and mutation of *CYCA2;1*, respectively (Fig. 5, F and G). As was observed in the experimental measurements, the simulations result in an increased hyponastic growth response for both *35S*::*CYCA2;1* and, to a slightly lesser extent, *cyca2;1*, except under the unrealistic scenario of exponential growth (Fig. 5D).

Taken together, our in silico model shows that reduced abaxial cell division decreases the amplitude of hyponastic growth. Furthermore, it demonstrates that when this mechanism is impaired by either constitutive *CYCA2;1* overexpression or by a knockout mutation, the hyponastic growth response becomes exaggerated, as was experimentally observed in both *35S*::*CYCA2;1* and *cyca2;1* (Fig. 2, A,G, and H).

DISCUSSION

Hyponastic growth is an adaptive response by which plants cope with adverse environmental conditions. The response is controlled by complex interactions between various phytohormones. However, since hyponastic growth induced by various independent environmental stimuli is highly similar in kinetics and amplitude, the signaling mechanisms likely converge downstream on specific functional molecular components that control the response (Van Zanten et al., 2010b). We aimed to identify unique molecular hyponastic growth regulators and isolated *EHY-D*, which has exaggerated amplitudes of leaf movement upon induction by ethylene, low light intensity, and high temperatures. Because *EHY-D* exhibited an enhanced response to each treatment investigated, the insertion likely affects a general downstream determinant of hyponasty. Our study shows that the core cell cycle regulator *CYCA2;1* was overexpressed in *EHY-D*. Several independent *A2-type CYCLIN* overexpression lines and mutants showed consistently altered hyponastic growth phenotypes (Fig. 2; Supplemental Figs. S3–S5), indicating that A2-type CYCLINs are important determinants of the hyponastic response.

Our results suggest that *A2-type CYCLIN*s operate in a specific branch of ethylene signaling that affects differential growth, but not hypocotyl elongation. We found that prolonged (6 h) ethylene treatment results in down-regulation of *A2-type CYCLIN*s in the petiole (Fig. 3, B and D). This down-regulation is initiated at least 3 h after the start of ethylene treatment, because up to this time point, *A2-type CYCLIN* transcription was unaffected (Fig. 2F). Since hyponastic growth is induced already within the first hour after ethylene application, transcriptional control of *A2-type CYCLIN*s likely does not control the induction of hyponastic growth.

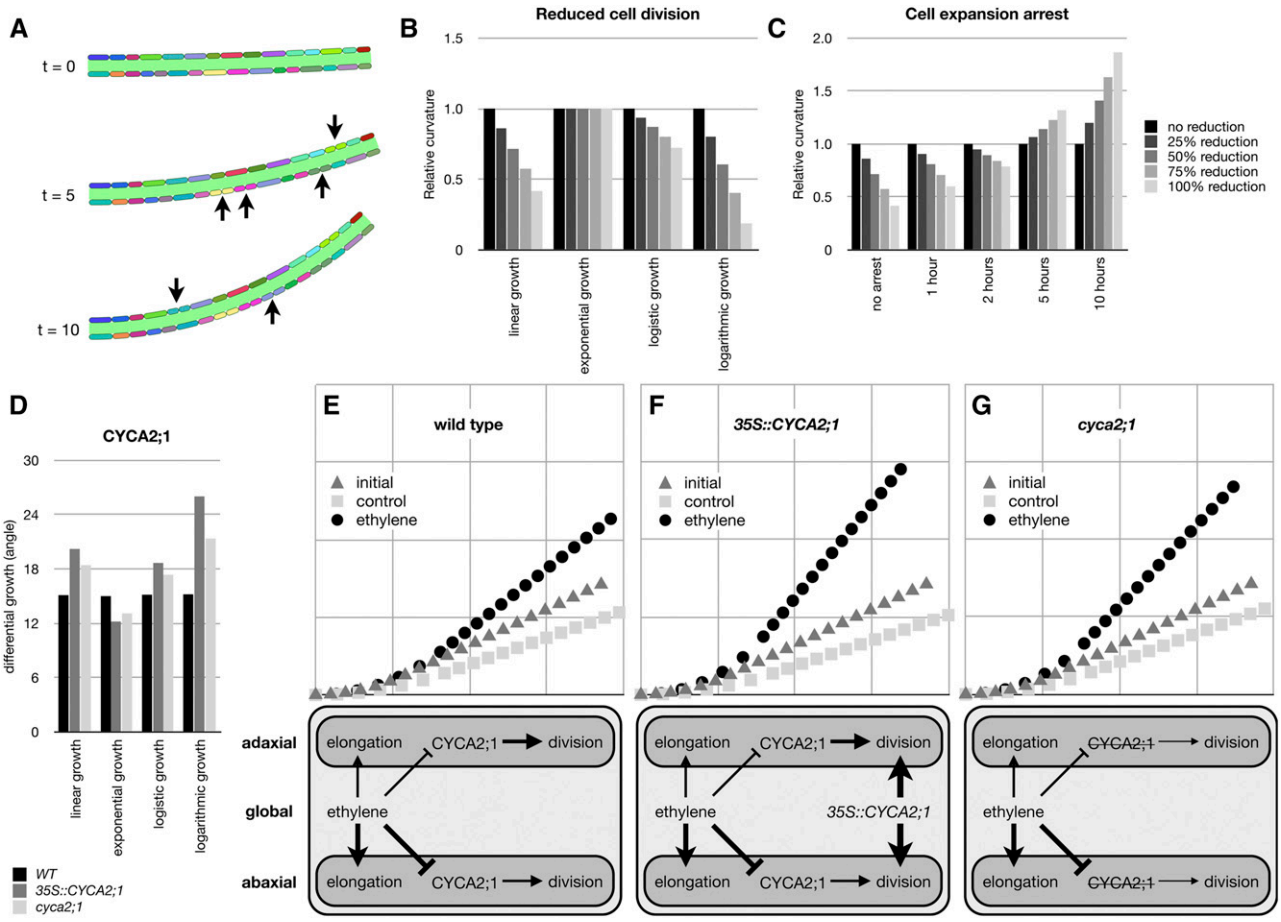

Figure 5. In silico model of ethylene-induced hyponastic growth. See Supplemental Texts S4 and S5 for details. A, Graphical representation of the model at different time points during a simulation of a wild-type Col petiole. The abaxial and adaxial cell layers are each represented by a single epidermal cell layer. Hyponastic growth during ethylene treatment (initiated at $t = 0$ h) is simulated for 10 h, during which both cell divisions (indicated with black arrows) and cell elongation are taking place. B, Effect of simulated ethylene treatment on petiole curvature for different levels (percentage) of abaxial reduction in cell division. Values are relative to petiole curvature without reduced abaxial cell division. Results are shown for linear, exponential, logistic, and logarithmic relations between cell length and cell expansion (see Supplemental Text S4). C, Effect of cell expansion arrest due to cell division on petiole curvature. Data are shown for linear cell expansion, values are relative to petiole curvature without reduced abaxial cell division and no cell expansion arrest. D, Simulation of ethylene-induced hyponastic growth in the wild type, *35S::CYCA2;1*, and *cyca2;1* background. Results are shown for linear, exponential, logistic, and logarithmic growth models. Values represent differential hyponastic growth relative to control treatment. The in silico model describes the cell expansion and divisions within the proximal part of the petiole, which is initially 3 mm but grows during the simulation, whereas the cells in the distal part (7 mm) were considered to have reached their final size (see Supplemental Text S5). E to G, Graphical representation of results shown in D for logarithmic growth. The symbols represent a side-on view of the petiole (see Supplemental Text S5) at $t = 0$ h (triangles) and after $t = 10$ h of either control treatment (squares) or ethylene treatment (circles). The scheme underneath E and F represents a simplification of the proposed mechanism that controls the amplitude of ethylene-induced hyponastic growth, as implemented in the in silico model for the wild-type, *35S::CYCA2;1*, and *cyca2;1* genetic background.

The promoter region of *CYCA2;1* contains eight ERF-binding ethylene responsive elements (Richard et al., 2001), implying that ethylene could control its transcription directly through ERF transcription factors that have the ethylene responsive element as their promoter targets.

Hyponastic Growth Does Not Depend on Ploidy Levels

A-type CYCLINs are expressed at the S-to-M transition of the mitotic cell cycle, prior to activation of B-type CYCLINs (Inzé and De Veylder, 2006) and are rate-limiting factors for entry in the mitotic cell phase (Burssens et al., 2000; Dewitte and Murray, 2003; Yu et al., 2003; Vanneste et al., 2011). Down-regulation of *CYCA2* levels causes a shift toward endoreduplication (Imai et al., 2006; Yoshizumi et al., 2006; Vanneste et al., 2011) and is associated with developmentally controlled cell cycle exit (Vanneste et al., 2011). This process is generally associated with differentiating cells undergoing cell expansion (Sugimoto-Shirasu and Roberts, 2003), e.g. in

Brassica oleracea petals (Kudo and Kimura, 2002). Consistently, ethylene has been shown to induce endoreduplication events in hypocotyls of *Cucumis sativus* and Arabidopsis (Gendreau et al., 1999; Dan et al., 2003). In our study, however, neither *CYCA2;1* overexpression nor ethylene application strongly affected ploidy levels in Arabidopsis petioles, which suggests that ethylene-induced hyponastic petiole growth is not regulated by *CYCA2*-mediated effects on the endocycle. This is in agreement with a previous study showing that petiole growth is independent of changes in ploidy levels (Kozuka et al., 2005). Possibly, the occurrence and role of endoreduplication in organ growth is less pronounced in petioles of mature plants than in hypocotyls of very young seedlings.

Differential Cell Proliferation Can Control Hyponastic Growth Amplitudes

Our finding that *CYCA2;1* overexpression or mutation causes an exaggerated hyponastic growth response is difficult to explain intuitively. Therefore, we developed an in silico model based on experimentally determined parameters, incorporating the effect of cell elongation and cell proliferation on petiole shape. It was critically important that the model predicted that a lack of differential cell proliferation between abaxial and adaxial petiole sides results in stronger hyponastic growth responses.

By combining cell length data and petiole shape, we were able to assess the influence of ethylene treatment and constitutive *CYCA2;1* expression on relative cell proliferation rates during hyponastic growth. This mathematical analysis showed that, in wild-type petioles, adaxial cell proliferation increases relative to abaxial cell proliferation during ethylene treatment. This can be caused by an increase in adaxial cell proliferation, a decrease in abaxial cell proliferation, or a combination of both. The scenario of decreased abaxial cell proliferation is the most likely explanation for the observed effect on hyponastic growth in the wild type, as this is in line with the observed down-regulation of *A2-type CYCLIN* expression following ethylene treatment. This is in accordance with a previous study indicating that ethylene can arrest the cell cycle by directly affecting core cell cycle components (Skirycz et al., 2011). Together, these data, combined with our mathematical analyses and the in silico model, suggest that the control of the amplitude of ethylene-induced hyponastic growth relies on a dual mechanism. Ethylene enhances cell elongation along the abaxial side of the petiole in wild-type plants, providing the tissue growth required for the upward movement of the petiole, while also down-regulating *CYCA2;1* and *CYCB1;1* expression, conceivably in a differential manner (see below), reducing abaxial cell proliferation. This reduced cell proliferation counteracts the effects of cell elongation, thereby attenuating the amplitude of the hyponastic response. When *CYCA2;1* is constitutively expressed, no differential inhibition of cell proliferation occurs, leading to an exaggerated hyponastic response. Our in silico model of hyponastic growth provides a proof of concept for this mechanism. Importantly, in addition to confirming the exaggerated response when *CYCA2;1* is constitutively expressed, the model also predicts that the same mechanism results in exaggerated hyponastic growth response when no CYCA2;1 is present. This was experimentally observed using *cyca2;1* knockout lines, which indeed show exaggerated hyponasty under ethylene treatment (Fig. 2, G and H).

The exact molecular mechanism by which ethylene installs differential cell proliferation between the abaxial and adaxial petiole side in ethylene-treated wild-type plants remains to be elucidated. Our work suggests that CYCA2;1 is critically involved. In this context, it is essential to consider the central role of distinct CDKs in complex with CYCLINs in controlling cell cycle checkpoints during cell proliferation. Besides the association with distinct CYCLINs whose levels are controlled at the level of transcription and protein stability, CDK activity is further fine tuned via interaction with proteins such as Kip-related proteins and regulatory phosphorylation events (Inzé and De Veylder, 2006; Polyn et al., 2015). Even if such components are involved, it remains unknown how the abaxial versus adaxial differentiation comes about, and this remains an important question for future studies.

The effect of ethylene on cell proliferation is complex and largely depends on the tissue context. On the one hand, ethylene was found to stimulate proliferation in the Arabidopsis root stem cell niche (Ortega-Martínez et al., 2007), in submergence-induced adventitious root growth in rice (Lorbiecke and Sauter, 1999), and in subsidiary cells of cucumber (*C. sativus*) hypocotyls and vascular tissues (Love et al., 2009; Etchells et al., 2012). On the other hand, in developing leaves, ethylene was found to suppress proliferation during mild osmotic stress (Skirycz et al., 2011), similar to the suppression in petioles presented in this work. Interestingly, this osmotic stress-induced cell cycle arrest is associated with regulation of CDKA;1 activity that does not involve EIN3-mediated transcriptional changes (Skirycz et al., 2011), suggesting that the effect of ethylene on differential regulation of proliferation in the petioles could involve nontranscriptional regulation. Consistently, we found that down-regulation of *A2-type CYCLIN*s in the petiole does not occur within 3 h of ethylene treatment (Fig. 2), whereas hyponastic growth is induced within the first hour after ethylene application.

The Bipartite Role for Ethylene in Hyponastic Response

In conclusion, we propose a dual role for ethylene in the mechanism regulating hyponastic growth. Ethylene (1) induces cell elongation in the abaxial petiole epidermal cells to power the upward leaf movement, and (2) inhibits the mitotic cell cycle, likely in part by affecting *CYCA2;1* expression, in the same tissue. An in silico model confirmed that such a mechanism can

explain the observed exaggerated hyponastic growth in both *35S::CYCA2;1* and *cyca2;1* null mutants. The dual role for ethylene found in this work adds to an increasing number of studies that indicate both growth stimulatory and inhibitory roles for ethylene in plant development, abandoning the classic idea of ethylene simply being a growth inhibitor. The hormone rather inhibits or stimulates growth in a subtle manner that integrates information from the environment together with developmental state and cellular identity of a tissue/organ (for review, see Pierik et al., 2006). This mechanism controls the magnitude of ethylene-induced hyponastic leaf movement in an effort to optimize plant performance under stressful conditions.

MATERIALS AND METHODS

Plant Material Growth Conditions

Arabidopsis (*Arabidopsis thaliana*) lines were from the Nottingham Arabidopsis Stock Centre (IDs between brackets) or were a gift of authors: Col (N1092), activation-tagged lines (Weigel et al., 2000; N21991, N23153), *ilp1-2*, *ILP1-1D* (Yoshizumi et al., 2006), *35S::CDKB1;1.N161* line 9.2 (Boudolf et al., 2009), *35S::SHN3* (Aharoni et al., 2004), *D-Box-CYCB1;1::GUS* (Colón-Carmona et al., 1999; Wildwater et al., 2005), *CYCA2;1::GUS* (Burssens et al., 2000; Vanneste et al., 2011), *CYCA2;2::GUS*, *CYCA2;3::GUS*, and *CYCA2;4::GUS* (Vanneste et al., 2011), *35S::TUBULIN ALPHA-6:GFP* (Ueda et al., 1999; gifted by Douglas Muench, University of Calgary, Canada), *cyca2;2-1* (SALK_121077; Yoshizumi et al., 2006), *cyca2;1-2* (SALK_123348; Vanneste et al., (2011), *cyca2;2-1* (GABI_120D03), *cyca2;3-1* (SALK_092515), and *cyca2;4-1* (SALK_070301). Double and triple mutants are based on crosses between these lines and are described in Vanneste et al. (2011). All alleles are representative knockouts.

Isolation of *35S::At3g25390* from the Arabidopsis TF ORF-Expression *ERF* ectopic expression library (Weiste et al., 2007) is described in Supplemental Materials and Methods S1. This line had an 11.7 ± 0.2 times higher expression of *SHN3* than the wild type, as determined by qRT-PCR.

Seeds were stratified at 4°C for 4 d, sown on a fertilized mixture of soil and perlite, and grown at 20°C, 70% (v/v) relative humidity, 200 μmol m^{-2} s^{-1} photosynthetically active radiation (9-h photoperiod) as described earlier (Millenaar et al., 2005). Thirty-day-old plants in stage 3.9 (Boyes et al., 2001) were used for all experiments, except for the hypocotyl elongation assay (below). One day before the start of the experiments, plants were transferred to the experimental setup with similar conditions to the growth chambers (Microclima 1750 growth cabinet; Snijders Scientific). To rule out effects of diurnal and circadian leaf movements, all treatments commenced 1.5 h after the start of the photoperiod.

To generate *35S::CYCA2;1* and *35S::CYCA2;2* plants, full-length complementary DNA was cloned through GATEWAY technology (Invitrogen) in pDONR221 and subcloned into pK2GW7,0 and pKGWFS7,0, respectively (Karimi et al., 2002). *35S::CYCA2;1* line Hmz B (Supplemental Figure S2) was used in all experiments involving *CYCA2;1* overexpression.

Real-Time Reverse Transcriptase-PCR and Histochemical β-Glucuronidase Staining

Real-time reverse transcriptase-PCR was conducted as described in Millenaar et al. (2005) and is described in detail in Supplemental Materials and Methods S1. Primers are shown in Supplemental Table S2 and in Richard et al. (2001), Mariconti et al. (2002), Yoshizumi et al. (2006), and Vanneste et al. (2011).

For histochemical GUS staining, tissues were harvested and placed briefly in 90% (v/v) ice-cold acetone and subsequently fixed and vacuum infiltrated with 10 mM MES, 0.3 M mannitol, and 0.3% (v/v) formaldehyde for 45 min. Tissues were rinsed in 100 mM buffer (50 mM $NaHPO_4$ + 50 mM Na_2HPO_4; pH 7.2). The histochemical reaction was performed by incubation in 1 mM 5-bromo-4-chloro-3-indolyl-β-glucuronic acid) in dimethyl sulfoxide for 24 h at 37°C. The tissues were cleared in an ethanol series of increasing concentrations (5%–90% [v/v]) and were either hand sectioned and directly observed or first embedded in Technovit 7100 (Kulzer) and dissected using a microtome. The resulting 200-μm sections were observed and photographed with an Olympus BX50 WI mounted with an Olympus DP 70 camera.

Ethylene, Low Light, and High Temperature Treatments

Ethylene (Hoek Loos) was applied to saturating (Polko et al., 2012b) concentrations (1.5 μL L^{-1}, except for the hyponastic growth kinetics experiment; see below) in continuous flow through and then vented away. The concentration was regularly checked by gas chromatography analysis. The control treatment was done in the same experimental cabinet. For leaf movement kinetics analysis, 5 μL L^{-1} ethylene was mixed with 70% (v/v) humidified air and applied to glass cuvettes containing one plant each at a flow rate of 75 L h^{-1} as described in Millenaar et al. (2005).

Low light intensity was induced by decreasing the photosynthetically active radiation level from 200 to 20 μmol m^{-2} s^{-1} by switching off lamps and by covering the plants with spectrally neutral shade cloth. This did not change light quality (checked with a LI-COR 1800 spectro-radiometer). Induction of high temperature was accomplished by moderating the program of the used growth cabinet. The 30°C threshold was reached after 22 min; 38°C was reached after 49 min.

Genetic Screen and Cloning of *EHY-D*

For details on the genetic screen that identified *EHY-D*, see Polko et al. (2012a). To facilitate easy and fast screening, we first checked if wild-type plants were able to exhibit a normal low light-induced hyponastic response after 6-h ethylene treatment and an overnight recovery. Ethylene-induced hyponastic growth was, as expected, quickly reversed by removing the ethylene source (Millenaar et al., 2005), and this treatment did not interfere with low light-induced hyponasty in the subsequent photoperiod (next day; Supplemental Fig. S10). In total, we screened 17,500 individual *Cauliflower mosaic virus* 35S enhancer (activation)-tagged (Weigel et al., 2000) vegetative plants in developmental stage 3.7 (Boyes et al., 2001). The plants were visually monitored for (1) petiole angle after 6 h of ethylene treatment and after overnight recovery, and (2) the petiole angle after 6-h low light treatment. To check the number of inserts, crosses were made between wild-type and the glufosinate ammonium (Basta)-resistant *EHY-D*. Self-pollinated F2 progeny seeds were subjected to Basta selection on agar plates containing 8 g L^{-1} plant agar (Duchefa), 0.22 g L^{-1} Murashige and Skoog (Duchefa), and 50 μg mL^{-1} DL-glufosinate ammonium (Basta/DL-phosphinotricin; Duchefa). After 3 weeks, survival ratios were scored. Thermal Asymmetric Interlaced-PCR was conducted to identify the T-DNA locus in *EHY-D* as described by Liu et al., (1995). For details, see Supplemental Materials and Methods S1.

Petiole Angle Measurements

Petiole angle kinetics was measured using an automated time-lapse camera system as described in Millenaar et al. (2005). Plants were placed in glass cuvettes with the petiole of study perpendicular to the axis of the camera. To facilitate measurement, leaves obscuring the petiole base were removed, and an orange paint droplet (Decofin Universal) was used to mark the petiole/lamina junction. This did not affect the response (data not shown). Digital images of two petioles per plant were taken every 10 min. Angles were measured between the marked point at the petiole/lamina junction and a fixed proximal point of the petiole, relative to the horizontal, using the KS400 (version 3.0) software package (Carl Zeiss Vision) and a custom-made macro. To enable continuous photography over the 24-h experimental period, no dark period was included during the experiments.

Plants used for measurements at fixed time points were manually photographed from the side. Angles were measured using ImageJ Software (Abramoff et al., 2004). Before further analysis, two petioles per plant were measured and an average was calculated. Statistical significance levels were determined using type-2 2-tailed Student's *t* test.

To rule out diurnal and/or circadian effects on petiole movement, a pairwise subtraction was performed on hyponastic growth data. Differential petiole angle describes a difference between the angle in control versus experimental conditions at each time point (Benschop et al., 2007). The new SE for the differential response was calculated by taking the square root from the summation of the two squared SEs. Initial petiole angles at t = 0 h of the *A2-type CYCLIN*-related lines are shown in Supplemental Table S1.

Cell Length Measurements and CMT Visualization

Cell length measurement of epidermal imprints of 1-cm-long petioles and visualization of arrangement of CMTs were performed as described in Polko

et al. (2012b). Cell lengths were quantified using a custom-made macro in KS400 software (Zeiss). Each cell was assigned to a 200-μm class, according to its position relative to the most proximal part of the petiole.

To visualize microtubules in the *35S::CYCA2;1* background, we crossed this line with *35S::TUA6:GFP* (Ueda et al., 1999). After 5 to 10 h of the ethylene/control treatment, CMTs of petiole epidermal cells were visualized using an inverted confocal laser-scanning microscope (Leica CS SPII, 63× C-apochromat objective, excitation wavelength of 488 nm, collecting at 505–530 nm for GFP emission). Petioles were divided in quadrants depending on their distance from the base, and the abaxial and adaxial sides were observed separately. Only CMT areas at least twice as long as the cell width were taken into account and grouped in categories relative to the long cell axis: transverse (0°), oblique 30°, oblique 60°, longitudinal (90°), and randomly oriented, according to Himmelspach and Nick (2001).

Ploidy Measurements

For ploidy measurements, two petioles or petiole segments of at least two plants (replicas) were snap frozen in liquid nitrogen, ground in extraction buffer (CyStain UV precise buffer P; Partec), diluted in a staining buffer (CyStain UV precise buffer P; Partec) containing 4′,6-diamidino-2-phenylindole, and analyzed on a Cytoflow ML flow cytometer (Partec).

Hypocotyl Elongation Assay and Ethylene Release Measurements

Hypocotyl elongation assay was conducted as described in Van Zanten et al. (2010a). Sterilized seeds were sown on petri dishes containing Murashige and Skoog-enriched plant agar (4 g L^{-1} plant agar [Duchefa], 0.22 g L^{-1} Murashige and Skoog [Duchefa], and different concentrations of ACC [Duchefa]). Plates were kept for 4 d at 4°C in dark. To induce germination, plates were transferred to 200 μmol m^{-2} s^{-1} light for 4 h and, subsequently, wrapped in aluminum-foil. Thereafter, the plates were left in darkness for 5 d at 20°C. Seedlings were photographed and hypocotyl length was measured using ImageJ software (Abramoff et al., 2004).

Ethylene release measurements were performed on 30-d-old plants, 1.5 ± 1 h after the start of the photoperiod, as described in Millenaar et al. (2005, 2009). Whole rosettes of about 300 mg were weighed and then placed in a syringe with a volume of 1.5 mL. Ethylene was allowed to accumulate in the syringe for 15 to 20 min. Subsequently, the air was analyzed on a gas chromatograph (GC955; Synspec). This short time frame prevented wound-induced ethylene production, which started to accumulate only after 20 min.

Mathematical Analysis of Cell Proliferation Rates

The mathematical model to predict cell proliferation rates is similar to the one described in Polko et al. (2012b). The background on secondary measurements of cell proliferation is explained in Supplemental Text S1, and parameters are in Supplemental Table S3. Petiole shape was quantified by fitting a function through the measured petiole angle data describing the proximal angle (petiole emergence from the shoot) and the distal angle (intersection of petiole and leaf blade). A smooth function was fitted to the measured cell lengths along the petiole to correct for variability. Given that along the adaxial side, hardly significant differences were found in cell lengths (Fig. 4A), the adaxial cell length data were fitted collectively to a single overarching function. In contrast, the abaxial cell length data showed significant differences in the proximal part (Fig. 4B) and were fitted for each individual data set independently. Since no significant differences in cell length were found in the distal part of the petiole, an extra constraint was added that required that the maximum cell length (in the distal part of the petiole) would be the same for the different data sets (Supplemental Table S3).

The curve describing petiole shape at $t = 0$ h was divided into 50 sections of 200 μm. An arc was fitted to each section, and by combining the curve of the arc with the function fitted to the measured cell lengths, the number of adaxial and abaxial cells per section could be calculated (see Supplemental Text S2 and Supplemental Table S3). The cell number per section at $t = 0$ h, combined with the functions describing the adaxial and abaxial cell lengths for the 10-h control and ethylene treatments, allowed calculation of predicted petiole shape after 10-h treatment for the null hypothesis, which assumes no cell proliferation during the treatments. Deviation from the predicted petiole shape to the observed shape allowed prediction of adaxial or abaxial cell proliferation (Supplemental Text S3). Since overall petiole elongation was not taken into account, the obtained cell proliferation rates represent relative rather than absolute values.

In Silico Model of Hyponastic Growth

In the in silico model, the (hyponastic) growth of the petiole was simulated for 10 h using 1-h time intervals. During each time step, cells expanded and/or divided. Cells could only divide after reaching a specified minimal length, after which the probability to divide existed and was evaluated at each time step. Simulations were initiated with a petiole that consisted of cells that were randomly selected from a population of in silico growing and dividing cells. This population was generated by simulating cell elongation and cell division for 10,000 time steps, starting from a single cell. All simulations were repeated 1,000 times (for parameters of all simulations, see Supplemental Table S4). For the results shown in Figure 5, D–G, the initial (abaxial and adaxial) length of the petiole was set such that the shape of the petiole resembles observations for the wild type at $t = 0$ h. Supplemental Text S5 discusses the relation between cell length and elongation for linear, exponential, logistic, and exponential growth, as well as the calculation of the petiole curvature (for results shown in Fig. 5, B and C) and differential (hyponastic) growth (for results shown in Fig. 5, D–G).

Supplemental Data

The following supplemental materials are available.

Supplemental Figure S1. Hyponastic response of plants ectopically expressing transcription factor *SHN3 ERF/AP2 B-6*.

Supplemental Figure S2. qRT-PCR analysis of *CYCA2;1* expression in independent *35S::CYCA2;1* transformants and *EHY-D*.

Supplemental Figure S3. Correlation analysis between *CYCA2;1* expression and amplitude of hyponastic growth in response to ethylene.

Supplemental Figure S4. Hyponastic response of *cyca2;1* mutants upon low light and high temperature treatment and expression of *A2-type CYCLIN*s.

Supplemental Figure S5. Hyponastic growth response of *35S:CYCA2;2-1* and *A2-type CYCLIN* double and triple mutant combination.

Supplemental Figure S6. Histochemical analysis of *A2-type CYCLIN* promoter activity in rosettes and petioles.

Supplemental Figure S7. Histochemical analysis of ethylene effects on *A2-cyclin* promoter activity in petioles.

Supplemental Figure S8. Effects of ethylene on endoreduplication in petioles.

Supplemental Figure S9. Ethylene-induced CMT reorientation in *35S::CYCA2;1* does not differ from the wild type.

Supplemental Figure S10. Ethylene treatment prior to low light treatment does not affect kinetics of low light-induced hyponastic growth.

Supplemental Table S1. Initial petiole angles at $t = 0$ h of *A2-type CYCLIN*-related mutants described in this work.

Supplemental Table S2. Primers used for real-time qRT-PCR.

Supplemental Table S3. Parameters used to profile cell proliferation rates.

Supplemental Table S4. Parameters used in the in silico model.

Supplemental Text S1. Indirect measurements of cell division and expansion rates.

Supplemental Text S2. Deriving the number of cells from petiole shape and cell lengths.

Supplemental Text S3. Profiling of cell proliferation along the petiole.

Supplemental Text S4. Influence of cell division on tissue growth.

Supplemental Text S5. Additional information for the in silico model of petiole.

Supplemental Materials and Methods S1.

ACKNOWLEDGMENTS

We thank Daan Weits (Utrecht University) for technical assistance and Takeshi Yoshizumi, Sari Osato (RIKEN Institute, Japan), Asaph Aharoni, Jianxin Shi (Weizmann Institute, Israel), Wolfgang Dröge-Laser (Universität Göttingen, Germany), and Douglas Muench (University of Calgary, Canada) for sharing materials.

Received March 5, 2015; accepted June 2, 2015; published June 3, 2015.

LITERATURE CITED

Abramoff MD, Magalhaes PJ, Ram SJ (2004) Image processing with ImageJ. Biophotonics International **11:** 36-42

Aharoni A, Dixit S, Jetter R, Thoenes E, van Arkel G, Pereira A (2004) The SHINE clade of AP2 domain transcription factors activates wax biosynthesis, alters cuticle properties, and confers drought tolerance when overexpressed in Arabidopsis. Plant Cell **16:** 2463–2480

Beemster GT, Baskin TI (1998) Analysis of cell division and elongation underlying the developmental acceleration of root growth in Arabidopsis thaliana. Plant Physiol **116:** 1515–1526

Benschop JJ, Millenaar FF, Smeets ME, van Zanten M, Voesenek LACJ, Peeters AJM (2007) Abscisic acid antagonizes ethylene-induced hyponastic growth in Arabidopsis. Plant Physiol **143:** 1013–1023

Boudolf V, Lammens T, Boruc J, Van Leene J, Van Den Daele H, Maes S, Van Isterdael G, Russinova E, Kondorosi E, Witters E, et al (2009) CDKB1;1 forms a functional complex with CYCA2;3 to suppress endocycle onset. Plant Physiol **150:** 1482–1493

Boyes DC, Zayed AM, Ascenzi R, McCaskill AJ, Hoffman NE, Davis KR, Görlach J (2001) Growth stage-based phenotypic analysis of Arabidopsis: a model for high throughput functional genomics in plants. Plant Cell **13:** 1499–1510

Bridge LJ, Franklin KA, Homer ME (2013) Impact of plant shoot architecture on leaf cooling: a coupled heat and mass transfer model. J R Soc Interface **10:** 20130326

Burssens S, de Almeida Engler J, Beeckman T, Richard C, Shaul O, Ferreira P, Van Montagu M, Inzé D (2000) Developmental expression of the Arabidopsis thaliana CycA2;1 gene. Planta **211:** 623–631

Cheniclet C, Rong WY, Causse M, Frangne N, Bolling L, Carde JP, Renaudin JP (2005) Cell expansion and endoreduplication show a large genetic variability in pericarp and contribute strongly to tomato fruit growth. Plant Physiol **139:** 1984–1994

Colón-Carmona A, You R, Haimovitch-Gal T, Doerner P (1999) Technical advance: spatio-temporal analysis of mitotic activity with a labile cyclin-GUS fusion protein. Plant J **20:** 503–508

Cox MC, Millenaar FF, Van Berkel YE, Peeters AJ, Voesenek LA (2003) Plant movement. Submergence-induced petiole elongation in Rumex palustris depends on hyponastic growth. Plant Physiol **132:** 282–291

Cox MCH, Benschop JJ, Vreeburg RAM, Wagemaker CA, Moritz T, Peeters AJM, Voesenek LACJ (2004) The roles of ethylene, auxin, abscisic acid, and gibberellin in the hyponastic growth of submerged *Rumex palustris* petioles. Plant Physiol **136:** 2948–2960, discussion 3001

Crawford AJ, McLachlan DH, Hetherington AM, Franklin KA (2012) High temperature exposure increases plant cooling capacity. Curr Biol **22:** R396–R397

Dan H, Imaseki H, Wasteneys GO, Kazama H (2003) Ethylene stimulates endoreduplication but inhibits cytokinesis in cucumber hypocotyl epidermis. Plant Physiol **133:** 1726–1731

de Wit M, Kegge W, Evers JB, Vergeer-van Eijk MH, Gankema P, Voesenek LACJ, Pierik R (2012) Plant neighbor detection through touching leaf tips precedes phytochrome signals. Proc Natl Acad Sci USA **109:** 14705–14710

Dewitte W, Murray JAH (2003) The plant cell cycle. Annu Rev Plant Biol **54:** 235–264

Dornbusch T, Michaud O, Xenarios I, Fankhauser C (2014) Differentially phased leaf growth and movements in *Arabidopsis* depend on coordinated circadian and light regulation. Plant Cell **26:** 3911–3921

Etchells JP, Provost CM, Turner SR (2012) Plant vascular cell division is maintained by an interaction between PXY and ethylene signalling. PLoS Genet **8:** e1002997

Gendreau E, Orbovic V, Höfte H, Traas J (1999) Gibberellin and ethylene control endoreduplication levels in the Arabidopsis thaliana hypocotyl. Planta **209:** 513–516

Grieneisen VA, Xu J, Marée AF, Hogeweg P, Scheres B (2007) Auxin transport is sufficient to generate a maximum and gradient guiding root growth. Nature **449:** 1008–1013

Guzmán P, Ecker JR (1990) Exploiting the triple response of *Arabidopsis* to identify ethylene-related mutants. Plant Cell **2:** 513–523

Harashima H, Schnittger A (2010) The integration of cell division, growth and differentiation. Curr Opin Plant Biol **13:** 66–74

Himmelspach R, Nick P (2001) Gravitropic microtubule reorientation can be uncoupled from growth. Planta **212:** 184–189

Imai KK, Ohashi Y, Tsuge T, Yoshizumi T, Matsui M, Oka A, Aoyama T (2006) The A-type cyclin CYCA2;3 is a key regulator of ploidy levels in Arabidopsis endoreduplication. Plant Cell **18:** 382–396

Inzé D, De Veylder L (2006) Cell cycle regulation in plant development. Annu Rev Genet **40:** 77–105

Karimi M, Inzé D, Depicker A (2002) GATEWAY vectors for Agrobacterium-mediated plant transformation. Trends Plant Sci **7:** 193–195

Keller MM, Jaillais Y, Pedmale UV, Moreno JE, Chory J, Ballaré CL (2011) Cryptochrome 1 and phytochrome B control shade-avoidance responses in Arabidopsis via partially independent hormonal cascades. Plant J **67:** 195–207

Keuskamp DH, Pollmann S, Voesenek LACJ, Peeters AJM, Pierik R (2010) Auxin transport through PIN-FORMED 3 (PIN3) controls shade avoidance and fitness during competition. Proc Natl Acad Sci USA **107:** 22740–22744

Koini MA, Alvey L, Allen T, Tilley CA, Harberd NP, Whitelam GC, Franklin KA (2009) High temperature-mediated adaptations in plant architecture require the bHLH transcription factor PIF4. Curr Biol **19:** 408–413

Kozuka T, Horiguchi G, Kim GT, Ohgishi M, Sakai T, Tsukaya H (2005) The different growth responses of the Arabidopsis thaliana leaf blade and the petiole during shade avoidance are regulated by photoreceptors and sugar. Plant Cell Physiol **46:** 213–223

Kudo N, Kimura Y (2002) Nuclear DNA endoreduplication during petal development in cabbage: relationship between ploidy levels and cell size. J Exp Bot **53:** 1017–1023

Lorbiecke R, Sauter M (1999) Adventitious root growth and cell-cycle induction in deepwater rice. Plant Physiol **119:** 21–30

Love J, Björklund S, Vahala J, Hertzberg M, Kangasjärvi J, Sundberg B (2009) Ethylene is an endogenous stimulator of cell division in the cambial meristem of Populus. Proc Natl Acad Sci USA **106:** 5984–5989

Liu YG, Mitsukawa N, Oosumi T, Whittier RF (1995) Efficient isolation and mapping of Arabidopsis thaliana T-DNA insert junctions by thermal asymmetric interlaced PCR. Plant J **8:** 457–463

Mariconti L, Pellegrini B, Cantoni R, Stevens R, Bergounioux C, Cella R, Albani D (2002) The E2F family of transcription factors from Arabidopsis thaliana. Novel and conserved components of the retinoblastoma/E2F pathway in plants. J Biol Chem **277:** 9911–9919

Millenaar FF, Cox MC, van Berkel YE, Welschen RA, Pierik R, Voesenek LACJ, Peeters AJM (2005) Ethylene-induced differential growth of petioles in Arabidopsis; analyzing natural variation, response kinetics, and regulation. Plant Physiol **137:** 998–1008

Millenaar FF, van Zanten M, Cox MCH, Pierik R, Voesenek LACJ, Peeters AJM (2009) Differential petiole growth in Arabidopsis thaliana: photocontrol and hormonal regulation. New Phytol **184:** 141–152

Moreno JE, Tao Y, Chory J, Ballaré CL (2009) Ecological modulation of plant defense via phytochrome control of jasmonate sensitivity. Proc Natl Acad Sci USA **106:** 4935–4940

Mullen JL, Weinig C, Hangarter RP (2006) Shade avoidance and the regulation of leaf inclination in Arabidopsis. Plant Cell Environ **29:** 1099–1106

Nakano T, Suzuki K, Ohtsuki N, Tsujimoto Y, Fujimura T, Shinshi H (2006) Identification of genes of the plant-specific transcription-factor families cooperatively regulated by ethylene and jasmonate in Arabidopsis thaliana. J Plant Res **119:** 407–413

Ortega-Martínez O, Pernas M, Carol RJ, Dolan L (2007) Ethylene modulates stem cell division in the Arabidopsis thaliana root. Science **317:** 507–510

Peña-Castro JM, van Zanten M, Lee SC, Patel MR, Voesenek LACJ, Fukao T, Bailey-Serres J (2011) Expression of rice SUB1A and SUB1C transcription factors in Arabidopsis uncovers flowering inhibition as a submergence tolerance mechanism. Plant J **67:** 434–446

Pierik R, Tholen D, Poorter H, Visser EJ, Voesenek LA (2006) The Janus face of ethylene: growth inhibition and stimulation. Trends Plant Sci **11:** 176–183

Pillitteri LJ, Bemis SM, Shpak ED, Torii KU (2007) Haploinsufficiency after successive loss of signaling reveals a role for ERECTA-family genes in Arabidopsis ovule development. Development **134:** 3099–3109

Polko JK, Pierik R, van Zanten M, Tarkowská D, Strnad M, Voesenek LACJ, Peeters AJM (2013) Ethylene promotes hyponastic growth through interaction with ROTUNDIFOLIA3/CYP90C1 in Arabidopsis. J Exp Bot **64:** 613–624

Polko JK, Temanni MR, van Zanten M, van Workum W, Iburg S, Pierik R, Voesenek LACJ, Peeters AJM (2012a) Illumina sequencing technology as a method of identifying T-DNA insertion loci in activation-tagged Arabidopsis thaliana plants. Mol Plant **5:** 948–950

Polko JK, van Zanten M, van Rooij JA, Marée AFM, Voesenek LACJ, Peeters AJM, Pierik R (2012b) Ethylene-induced differential petiole growth in Arabidopsis thaliana involves local microtubule reorientation and cell expansion. New Phytol **193:** 339–348

Polyn S, Willems A, De Veylder L (2015) Cell cycle entry, maintenance, and exit during plant development. Curr Opin Plant Biol **23:** 1–7

Potuschak T, Lechner E, Parmentier Y, Yanagisawa S, Grava S, Koncz C, Genschik P (2003) EIN3-dependent regulation of plant ethylene hormone signaling by two arabidopsis F box proteins: EBF1 and EBF2. Cell **115:** 679–689

Rauf M, Arif M, Fisahn J, Xue GP, Balazadeh S, Mueller-Roeber B (2013) NAC transcription factor SPEEDY HYPONASTIC GROWTH regulates flooding-induced leaf movement in *Arabidopsis*. Plant Cell **25:** 4941–4955

Richard C, Granier C, Inzé D, De Veylder L (2001) Analysis of cell division parameters and cell cycle gene expression during the cultivation of Arabidopsis thaliana cell suspensions. J Exp Bot **52:** 1625–1633

Roeder AHK, Chickarmane V, Cunha A, Obara B, Manjunath BS, Meyerowitz EM (2010) Variability in the control of cell division underlies sepal epidermal patterning in Arabidopsis thaliana. PLoS Biol **8:** e1000367

Savaldi-Goldstein S, Peto C, Chory J (2007) The epidermis both drives and restricts plant shoot growth. Nature **446:** 199–202

Skirycz A, Claeys H, De Bodt S, Oikawa A, Shinoda S, Andriankaja M, Maleux K, Eloy NB, Coppens F, Yoo SD, et al. (2011) Pause-and-stop: the effects of osmotic stress on cell proliferation during early leaf development in *Arabidopsis* and a role for ethylene signaling in cell cycle arrest. Plant Cell **23:** 1876–1888

Sugimoto-Shirasu K, Roberts K (2003) "Big it up": endoreduplication and cell-size control in plants. Curr Opin Plant Biol **6:** 544–553

Ueda K, Matsuyama T, Hashimoto T (1999) Visualization of microtubules in living cells of transgenic Arabidopsis thaliana. Protoplasma **206:** 201-206

Vandepoele K, Raes J, De Veylder L, Rouzé P, Rombauts S, Inzé D (2002) Genome-wide analysis of core cell cycle genes in Arabidopsis. Plant Cell **14:** 903–916

Vanneste S, Coppens F, Lee E, Donner TJ, Xie Z, Van Isterdael G, Dhondt S, De Winter F, De Rybel B, Vuylsteke M, et al (2011) Developmental regulation of CYCA2s contributes to tissue-specific proliferation in Arabidopsis. EMBO J **30:** 3430–3441

van Zanten M, Basten Snoek L, van Eck-Stouten E, Proveniers MCG, Torii KU, Voesenek LACJ, Peeters AJM, Millenaar FF (2010a) Ethylene-induced hyponastic growth in Arabidopsis thaliana is controlled by ERECTA. Plant J **61:** 83–95

Van Zanten M, Pons TL, Janssen JAM, Voesenek LACJ, Peeters AJM (2010b) On the relevance and control of leaf angle. Crit Rev Plant Sci **29:** 300-316

van Zanten M, Voesenek LACJ, Peeters AJM, Millenaar FF (2009) Hormone- and light-mediated regulation of heat-induced differential petiole growth in Arabidopsis. Plant Physiol **151:** 1446–1458

Vasseur F, Pantin F, Vile D (2011) Changes in light intensity reveal a major role for carbon balance in Arabidopsis responses to high temperature. Plant Cell Environ **34:** 1563–1576

Weigel D, Ahn JH, Blázquez MA, Borevitz JO, Christensen SK, Fankhauser C, Ferrándiz C, Kardailsky I, Malancharuvil EJ, Neff MM, et al (2000) Activation tagging in Arabidopsis. Plant Physiol **122:** 1003–1013

Weiste C, Iven T, Fischer U, Oñate-Sánchez L, Dröge-Laser W (2007) In planta ORFeome analysis by large-scale over-expression of GATEWAY-compatible cDNA clones: screening of ERF transcription factors involved in abiotic stress defense. Plant J **52:** 382–390

Wildwater M, Campilho A, Perez-Perez JM, Heidstra R, Blilou I, Korthout H, Chatterjee J, Mariconti L, Gruissem W, Scheres B (2005) The RETINOBLASTOMA-RELATED gene regulates stem cell maintenance in Arabidopsis roots. Cell **123:** 1337–1349

Yoshizumi T, Tsumoto Y, Takiguchi T, Nagata N, Yamamoto YY, Kawashima M, Ichikawa T, Nakazawa M, Yamamoto N, Matsui M (2006) INCREASED LEVEL OF POLYPLOIDY1, a conserved repressor of *CYCLINA2* transcription, controls endoreduplication in *Arabidopsis*. Plant Cell **18:** 2452–2468

Yu Y, Steinmetz A, Meyer D, Brown S, Shen WH (2003) The tobacco A-type cyclin, *Nicta;CYCA3;2*, at the nexus of cell division and differentiation. Plant Cell **15:** 2763–2777

Supplemental Figures

Figure S1

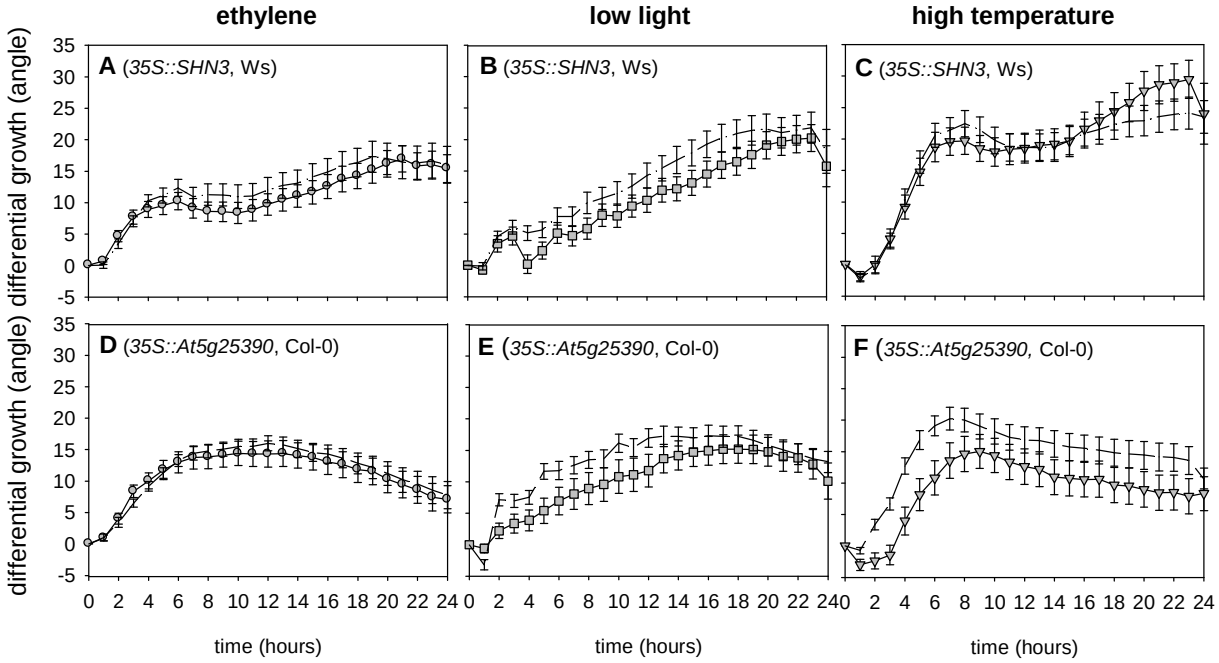

Figure S1. Hyponastic response of plants ectopically expressing transcription factor *SHN3 ERF/AP2 B-6.* A-C, Response to ectopic expression of *SHN3* (gray symbols) in the Wassilewskija (Ws) genetic background (dash-dotted lines) and D-F, *SHN3* (35S::At5g25390; gray symbols) in the Col (dashed lines) genetic background upon: A,D, ethylene (5 µl l^{-1}; circles), B,E, low-light (20 µmol m^{-2} s^{-1}; squares) and C,F, high temperature (38°C; triangles) treatment. Angles resulted from pair-wise subtraction (Benschop *et al.*, 2007). Error bars are SEM; n>10.

Figure S2

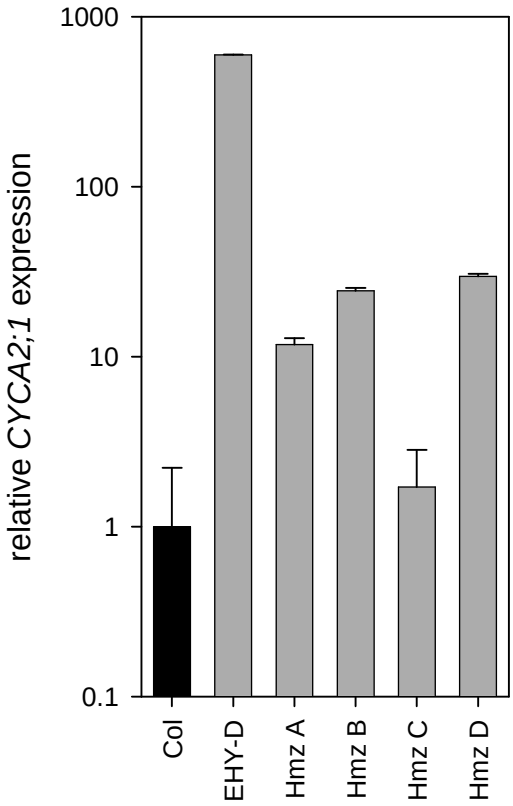

Figure S2. qRT-PCR analysis of *CYCA2;1* expression in independent *35S::CYCA2;1* transformants and *EHY-D.* Expression levels were assayed in homozygous plants (gray bars) and normalized to 1 for Col wild-type (black bar), n≥4; Standard errors are SEM. Transgenic line Hmz B was further characterized and is referred to as *35S::CYCA2;1* throughout the manuscript.

Figure S3

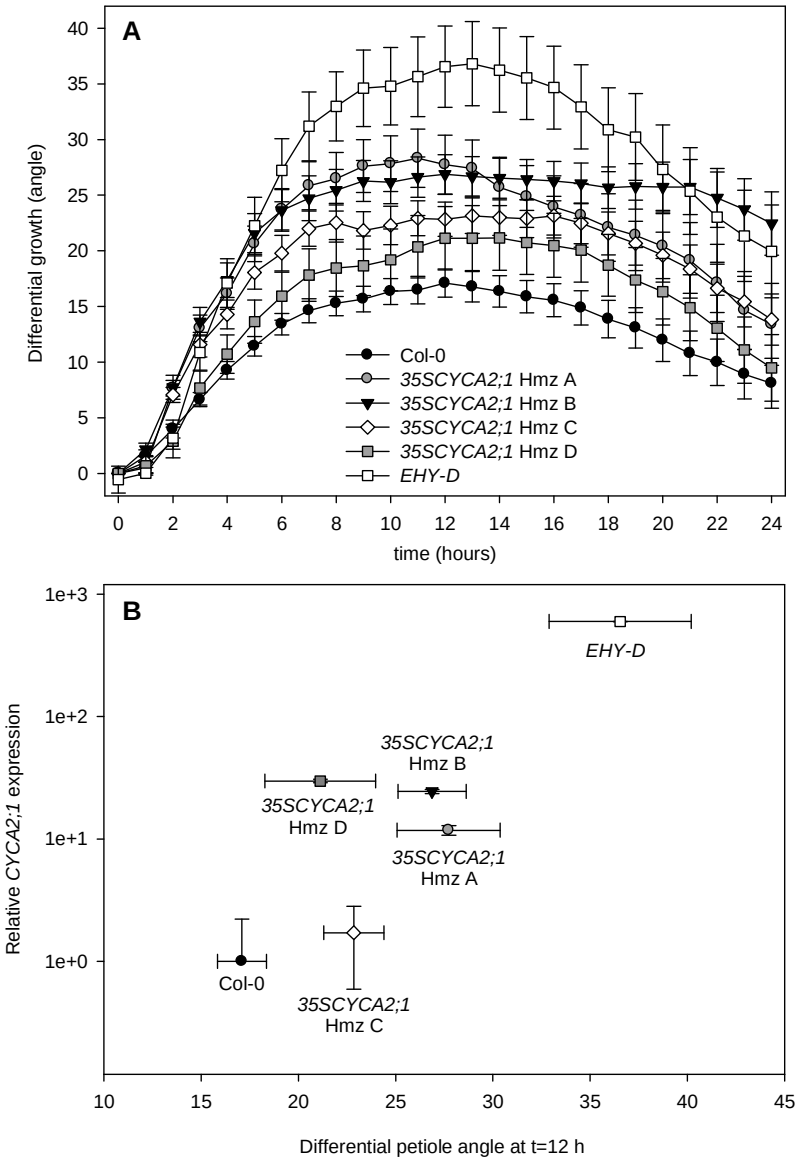

Figure S3. Correlation analysis of *CYCA2;1* expression and amplitude of hyponastic growth in response to ethylene. A, Hyponastic response of Col wild-type (black circles) and four independent *35S::CYCA2;1* overexpression lines (see Fig. S2 for details), Hmz A (gray circles), Hmz B (black triangles), Hmz C (white diamonds), Hmz D (gray squares) and *EHY-D* (white squares) upon ethylene (5 µl l^{-1}) treatment. Angles resulted from pair-wise subtraction (Benschop *et al.*, 2007). Error bars are SEM; n>10. B, Correlation between *CYCA2;1* expression (Y-axis; See Fig. S2) and differential (hyponastic) petiole angle at t=12 h of ethylene treatment. For details see panel A. Error bars are SEM; n>10. Note that Y-axis is logarithmic scale.

Figure S4

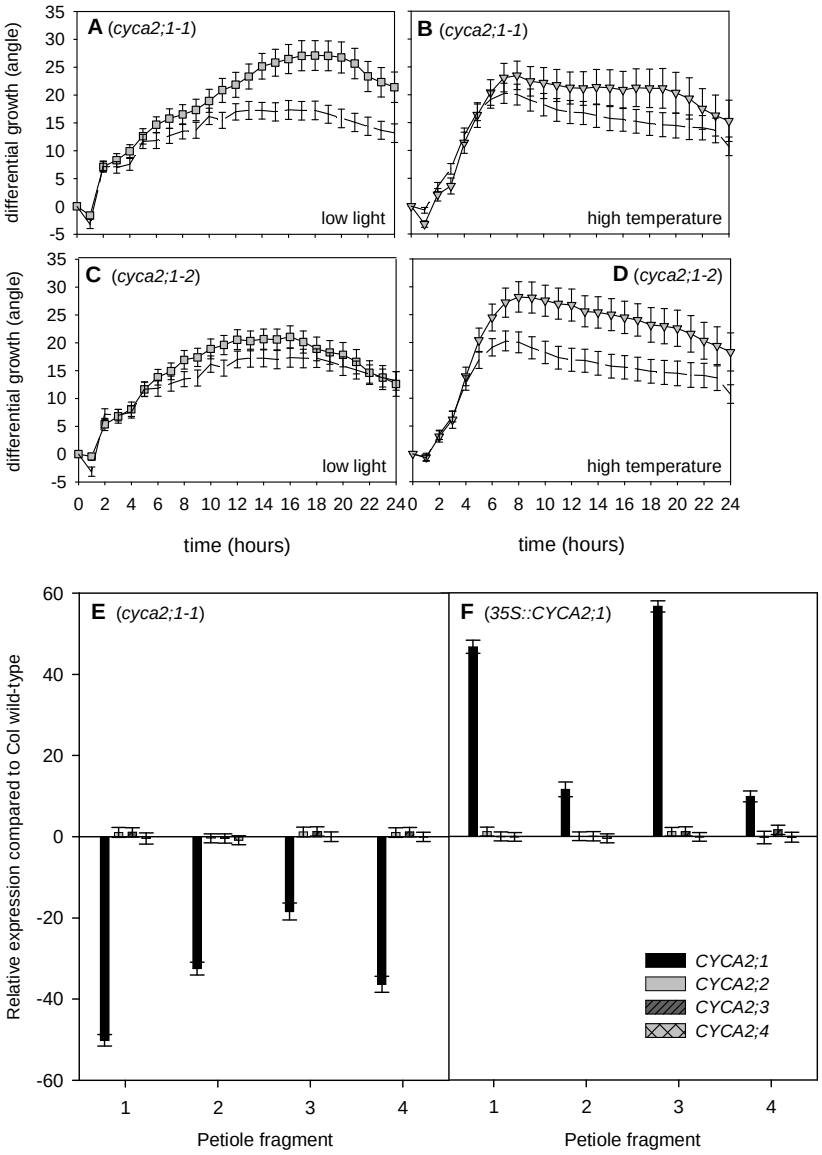

Figure S4. Hyponastic response of *cyca2;1* mutants upon low light and high temperature treatment and expression of *A2-type CYCLINS*. Response kinetics of A,B, *cyca2;1-1* and C,D, *cyca2;1-2* insertion mutants and Col wild-type (dashed lines) upon A,C, low light (squares) and B,D, high temperature (triangles) treatment. Angles resulted from pair-wise subtraction. Error bars are SEM; n>10. For details see legend Fig. S1. E,F, qRT-PCR expression analysis of *A2-type CYCLINS* in E, *cyca2;1-2* knockout mutant and F, *35S::CYCA2;1* Hmz B overexpression line in petiole quarters (see Fig. 3 for details). Expression levels of qRT-PCR experiments are relative to Col wild-type, n=3; Standard errors are SEM.

Figure S5

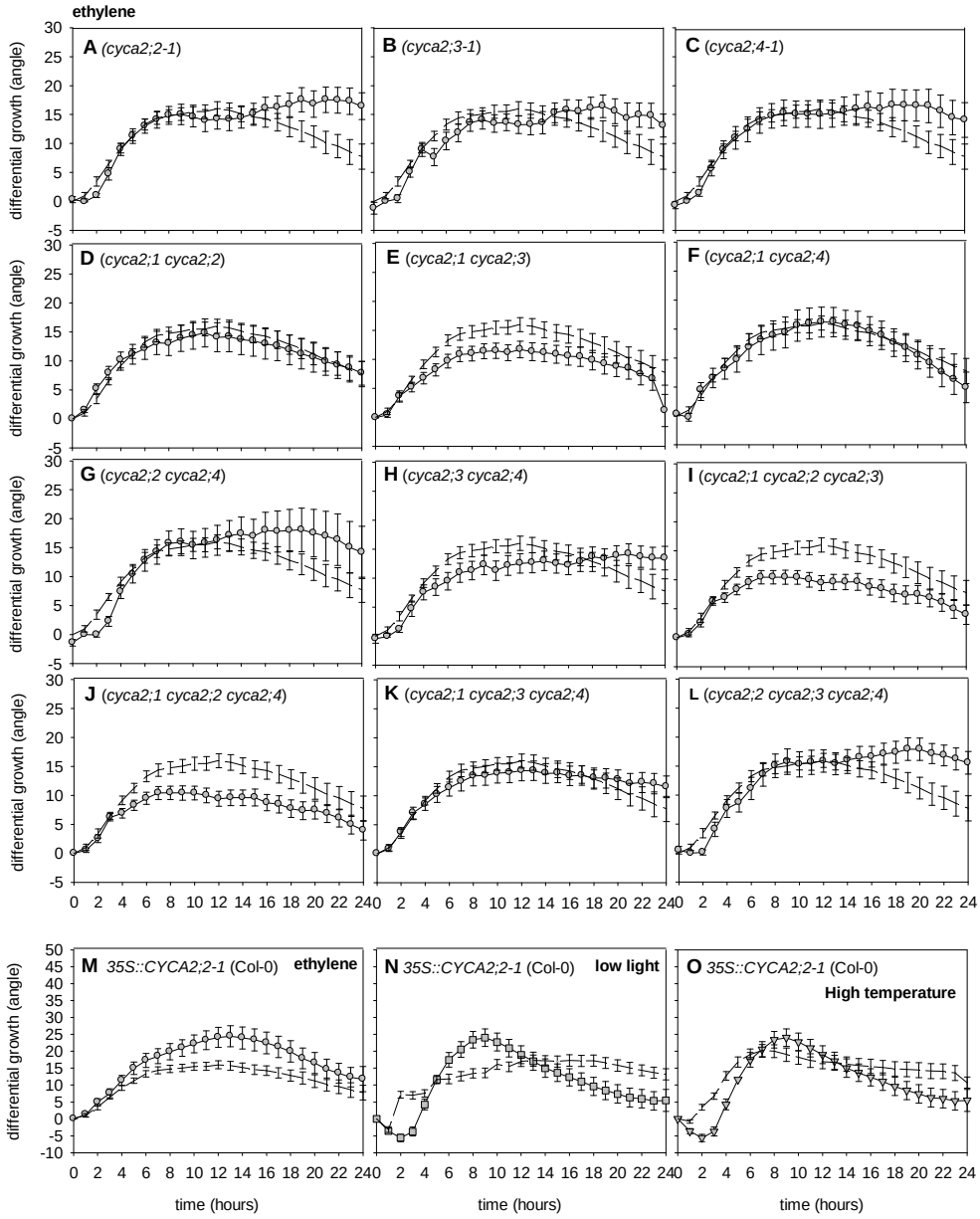

Figure S5 Hyponastic growth response of A2-type CYCLIN single mutants, double- and triple mutant combinations, and *35S:CYCA2;2-1*. Hyponastic growth response of single *A2-type CYCLIN* mutants and double- and triple mutant combinations (circles) compared to wild-type (dashed lines) upon ethylene (5 µl l^{-1}) treatment. M-O, hyponastic growth response kinetics of *35S:CYCA2;2-1* upon M, ethylene (5 µl l^{-1}; circles); N, low light (squares) and O, high temperature treatment (triangles) compared to Col wild-type (dashed lines). Angles resulted from pair-wise subtraction. Error bars are SEM; n>10. For details see legend Fig. S1.

Figure S6

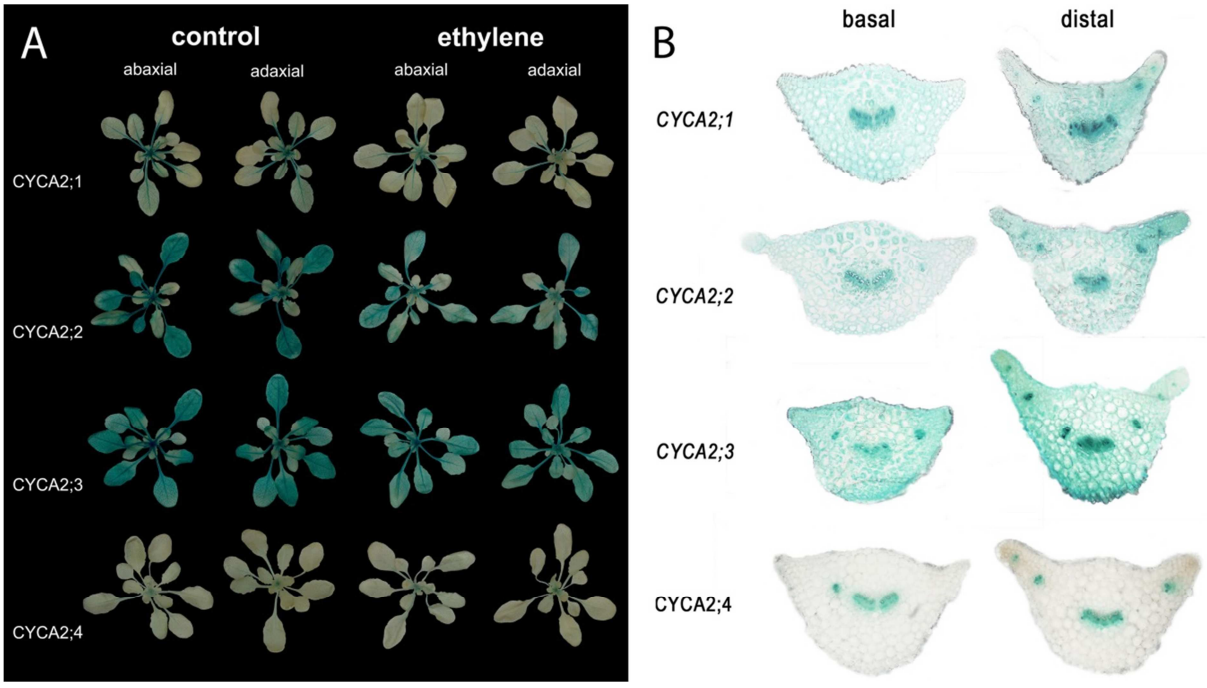

Figure S6. Histochemical analysis of *A2-Cyclin* activity in rosettes and petioles. A, Plants carrying individual *A2-type CYCLIN* family promoters fused to the β-glucuronidase (GUS) reporter gene. Plants were either kept in control (air) conditions or ethylene conditions and were photographed from the abaxial (left) and adaxial side (right). B, Histochemical staining of basal and distal transverse sections of control-treated (air) petioles in the developmental stage (~1 cm in length) as used throughout this study. Note that these hand-cut sections are not indicative for quantitative promoter activity (but see Figure 3B in the main text).

Figure S7

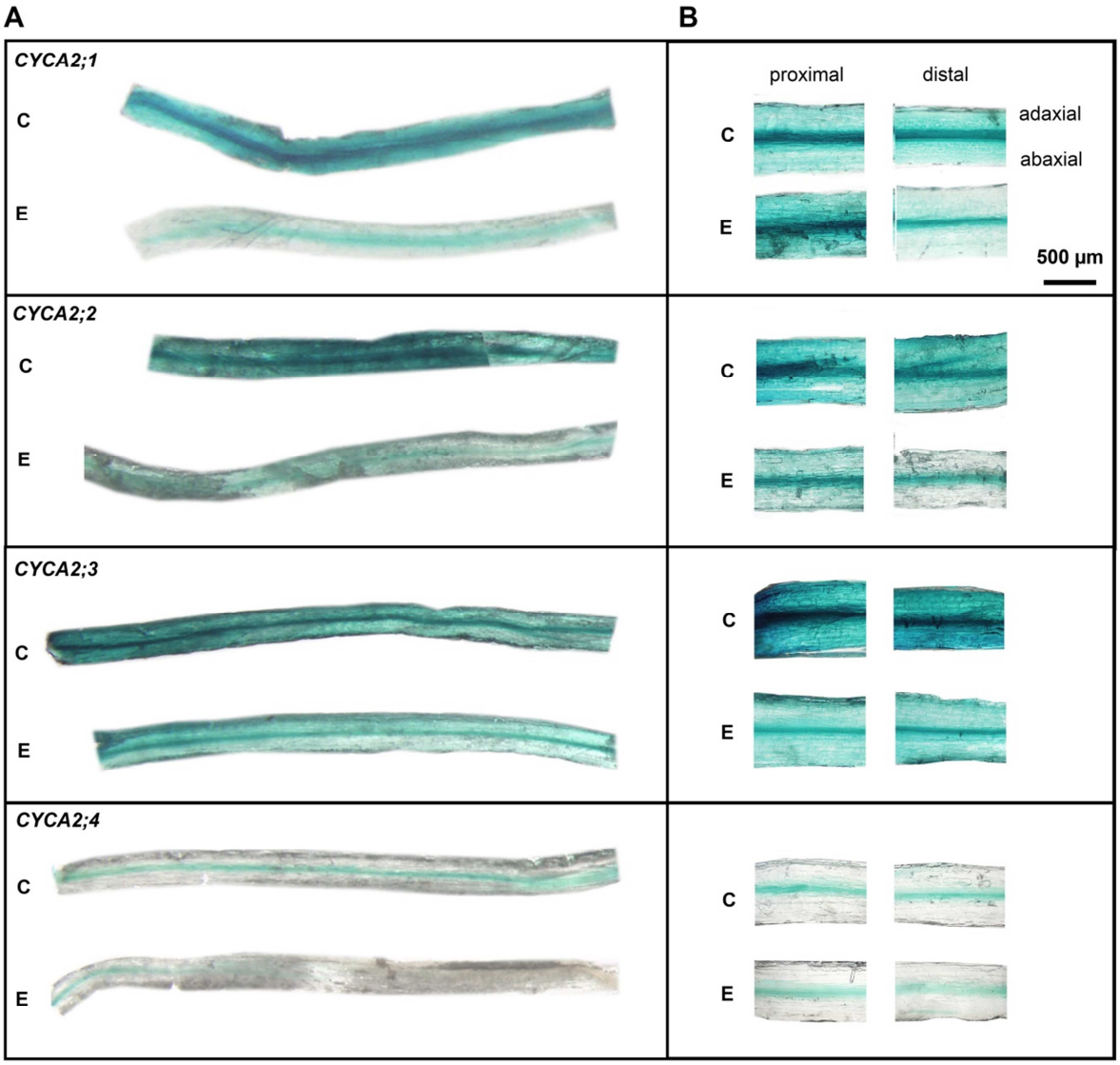

Figure S7. Histochemical analysis of ethylene effects on *A2-Cyclin* activity in petioles. A, representative 200 µm thick histochemically stained petioles of plants carrying individual *A2-type CYCLIN* family promoters fused to the β-glucuronidase (GUS) reporter gene. Plants were treated with air (6 h, control C) or ethylene (6 h, E). B, Close-up of representative proximal and distal 200 µm thick petiole sections of plants treated with air (6 h, control C) or ethylene (6 h, E). Scale bar (for panel B only) represents 500 µm.

Figure S8

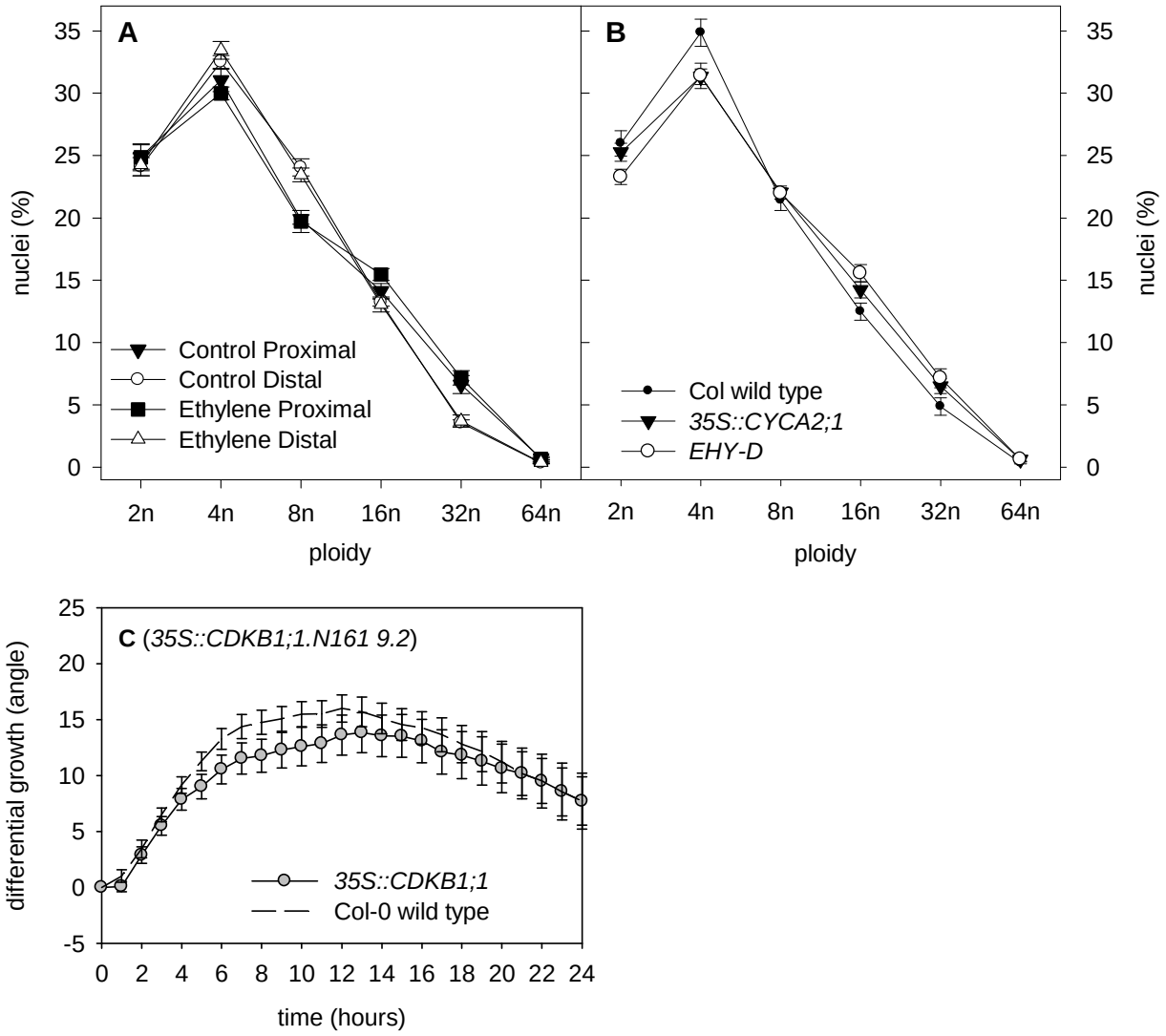

Figure S8. Effects of ethylene on endoreduplication in petioles. A,B, Fraction of nuclei with the indicated ploidy level (%) in A, wild-type nuclei derived from the proximal (closed symbols) and most distal (open symbols) petiole quarter, before (0 h; circles) and after 6 h ethylene (squares) or control (air; triangles) treatment and B, petioles of *EHY-D* (open circles), *35S::CYCA2;1* (closed triangles), and the wild-type (closed circles). Error bars are SEM; n=6-8. C, Kinetics of hyponastic growth in *35S::CDKB1;1.N161 line 9.2* (gray circles) in the Col background (dashed lines), upon ethylene treatment. Error bars are SEM; n>10. For details see legend Fig. S1.

Figure S9

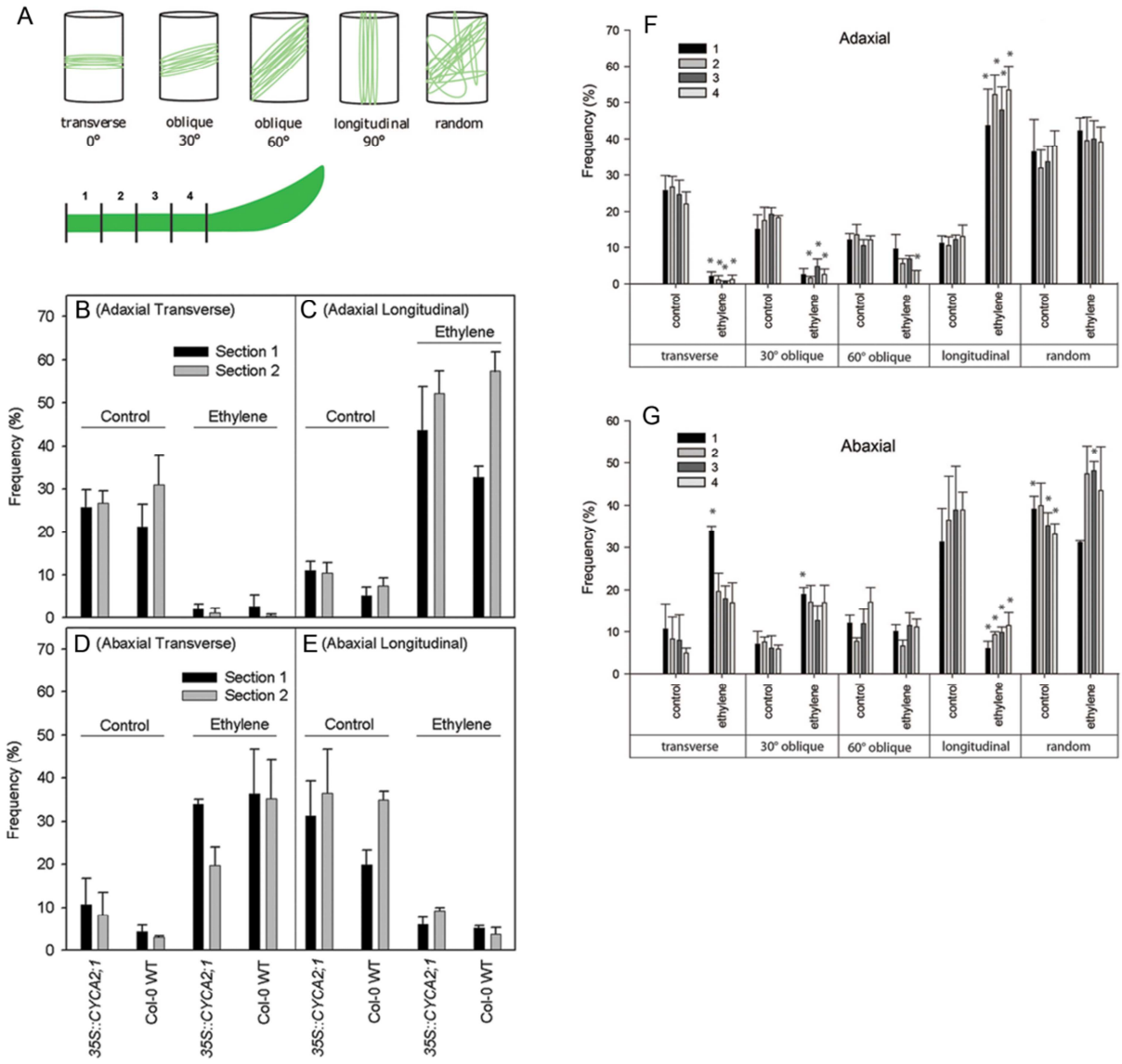
A
transverse 0°
oblique 30°
oblique 60°
longitudinal 90°
random
1
2
3
4
B (Adaxial Transverse)
C (Adaxial Longitudinal)
D (Abaxial Transverse)
E (Abaxial Longitudinal)
Section 1
Section 2
Control
Ethylene
Frequency (%)
35S::CYCA2;1
Col-0 WT
F
Adaxial
G
Abaxial
control
ethylene
transverse
30° oblique
60° oblique
longitudinal
random

Figure S9. Ethylene-induced CMT reorientation in *35S::CYCA2;1* does not differ from the wild-type. A, Schematic illustration of cortical microtubules (CMT) orientation types according to Polko *et al.* (2012a) (top) and illustration of petiole quadrants used in this study (bottom). Note that transverse orientation corresponds with longitudinal cell expansion. B-E, CMT orientation in *35::CYCA2;1* and the wild-type in the B,D, transverse and C,E, longitudinal orientation in petiole epidermal cells of petiole fragments (see panel A) #1 (black) and #2 (gray) at the B,C, adaxial and D,E, abaxial side, upon 5-10 h ethylene treatment or control conditions. Note that the pattern of (re)orientation is highly similar between *35:CYCA2;1* and the wild-type. F,G, Complete representation of CMT orientation quantified in this study in *35S::CYCA2;1* petiole epidermal cells upon 5 to 10 h ethylene treatment at the F, adaxial and G, abaxial side of the petiole. Significance levels; 2-tailed Student's t-test; between the frequency in control and ethylene treated plants. *$p<0.05$. All data points are averages (n=3) of areas representing categories of CMT arrangement. Error bars are SEM.

Figure S10

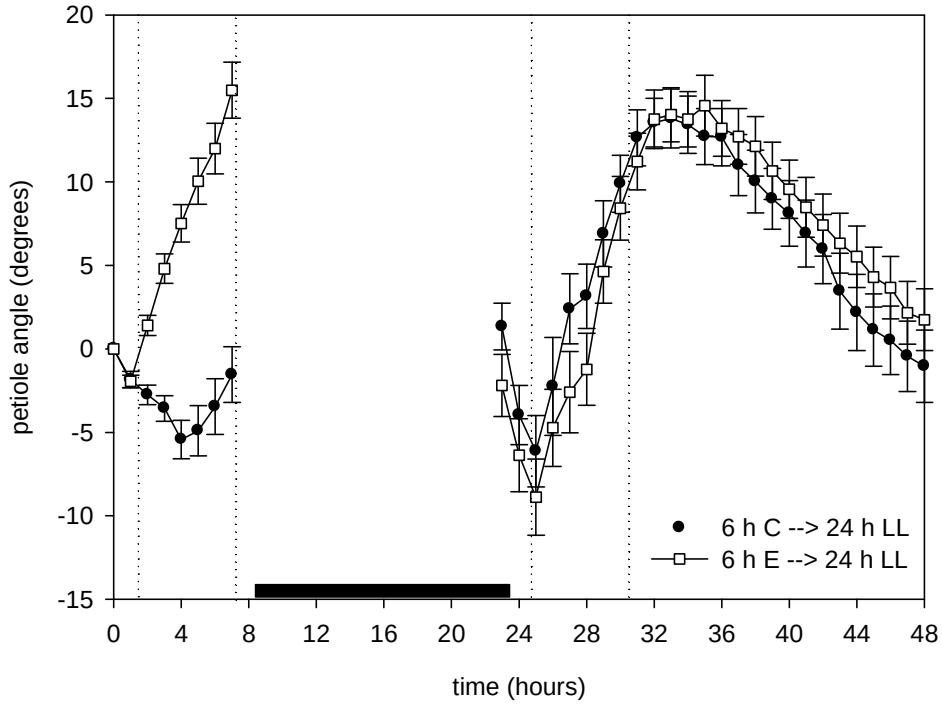

Figure S10. Ethylene treatment prior to low light treatment does not affect kinetics of low light-induced hyponastic growth. Col plants subjected to 6 h ethylene treatment (E; started at 0h; 5 µl l^{-1}; white squares) or air control (black circles), followed the next day by low light treatment (LL; started at 24 h; 20 µmol m^{-2} s^{-1}). Petiole angles were normalized to 0 degrees to allow comparison. The dark period is represented by the black horizontal bar. Error bars are SEM; n>10.

Supplemental Methods S1

Isolation of *35S::At3g25390* (*SHN3*) in the Col genetic background

DNA was isolated of 200 pooled (5 individuals per pool) plants of set 'IV' of the *At*TOTF-Ex ERF ectopic expression library, which contains a mixture of 25 independent 35S CaMV promoter tagged *ERF* lines, including *35S::At5g25390* (Weiste *et al.*, 2007). Pools were screened for the presence of *35S::At5g25390* by standard PCR procedure, using a forward primer designed to span part of the GATEWAY vector T-DNA, the start codon and a small *At5g25390* specific sequence (5'-CAGGCTTCATGGTACATTCG-3') and a *At5g25390* gene-specific reverse primer (5'-TGAACCGTTCGATTTGATGA-3'). Individual plants of pools from which a product of the expected size was obtained, were checked with the same primer combination and with vector specific primers that span the recombination sites (5'-GGGGACAAGTTTGTACAAAAAAGCAG-3', 5'-CGTATGGATAACCCCATCAACCAC-3'), to check for the number of inserts. To confirm the presence of *35S::At5g25390,* PCR fragments of lines that contained one insert of the expected size were sequenced using the primer: 5'-CAGGCTTCATGGTACATTCG-3' (Macrogen, Seoul, South-Korea). The confirmed lines were grown on selective agar-plates containing 8 g l^{-1} plant agar (Duchefa, Haarlem, The Netherlands), 0.22 g l^{-1} Murashige-Skoog (Duchefa) and 50 µg ml^{-1} DL-Glufosinate ammonium (BASTA/DL-phosphinotricin; Duchefa). To isolate homozygous *35S::At5g25390* lines, survival rates were scored after three weeks. Thereafter, *At5g25390* overexpression was determined by Real-Time qRT-PCR using the primers: 5'-GGGTCAAAAACGAGTCCAAA-3'; 5'-CGCCATTTGATCATCTTCCT-3'.

TAIL-PCR

TAIL-PCR was conducted to identify the T-DNA locus in *EHY-D* as described by Liu *et al.* (1995). Genomic-DNA was isolated using Nucleon Phytopure DNA extraction kit, (GE Healthcare/Amersham; Den Bosch, The Netherlands). Integrity of the DNA was checked by amplification of Actin (At5g09810) using the primers: 5'-GCATCATCACAAGCATCCTAA-3' and 5'-TTCGTGGTGGTGCGTTTGTT-3'. Subsequent TAIL-PCR was conducted using the degenerate primer: AD2; 5'-NGTCGASWGANAWGAA-3', TTCWTNTCWSTCGACN; (Liu *et al.*, 1995) in combination with nested

primers from the Left-border: 5'-ATCTAAGCCCCCATTTGGAC-3' (primary PCR); 5'-TAACGCTGCGGACATCTACA-3' (secondary PCR); 5'-CGGACATGAAGCCATTTACA-3' (tertiary PCR). PCR products were separated on agarose-gel and excised bands containing DNA purified using a GFX-spin column (GE Healthcare/Amersham) and subjected to direct sequencing (Macrogen, Seoul, South-Korea) using the tertiary PCR primer.

Real-time quantitative reverse transcriptase-PCR

Real-time quantitative reverse transcriptase-PCR was conducted as described in Millenaar *et al.* (2006). Tissues were harvested and snap-frozen in liquid nitrogen. For one RNA sample (fragments of) eight petioles of four plants were pooled. RNA was isolated using the RNeasy Plant Mini Kit (Qiagen, Leusden, The Netherlands). Genomic DNA was removed using the DNA-Free kit (Ambion, Cambridgeshire, United Kingdom). Superscript III RNaseH$^-$ Reverse Transcriptase (Invitrogen, Breda, The Netherlands). Random-Hexamer Primers, were used for cDNA synthesisis. Real-Time RT-PCR reactions were performed on a MyiQ Single-Color Real-Time PCR Detection System and Software using iQ SYBR Green Supermix Fluorescein (Bio-Rad laboratories, Veenendaal, The Netherlands). Primers for *EHY-D* T-DNA flanking genes are described in Supplemental Table S2. Primers for *A2-CYCLIN* genes and cell cycle-specific genes were custom designed or are derived from Richard *et al.* (2001), Mariconti *et al.* (2002) and Yoshizumi *et al.* (2006)**.** Relative mRNA values were calculated using the comparative cycle threshold (C_t) method described by Livak and Schmittgen, (2001), expressing mRNA values relative to *ß-Tubulin-6* (At5g12250, 5'-ATAGCTCCCCGAGGTCTCTC-3', 5'-TCCATCTCGTCCATTCCTTC-3' (Czechowski *et al.*, 2004)).

.

Text S1. Indirect measurements of cell division and expansion rates

Ideally, cell division and expansion are studied by following each individual cell over time. In this way cell division and expansion can be quantified with both temporal and spatial resolution. However, following individual plant cells over time is far from trivial, since imaging and measuring cells within a living plant tissue is often invasive, resulting in damaging or killing the tissue. Consequently, cells are often measured at only a single time point, which makes it impossible to directly measure cell division and expansion.

When the development of a tissue is comparable between specimens, it is still possible to study cell elongation and division by looking at average cell size and number in different tissues at different time points. In this case it is important to realize that observed changes in average cell length are influenced by both cell expansion, which has a positive effect on the average observed cell length, and cell division, which has a negative effect on the average observed cell length.

When the observation window of an experiment includes the whole tissue (or an identifiable section of the tissue), it is possible to use the observed cell expansion and the observed change in cell number to calculate cell division and cell expansion rates (Fig. with text S1A). The absolute cell division rate is then given by the increase in average number of cells over time (assuming no cell death) and the actual cell expansion can be obtained by correcting the observed average cell expansion for the cell division rate using a straightforward calculation.

When (due to experimental constraints) the observation window contains only part of the tissue, cell division and elongation rates cannot be extracted from the data so straightforwardly (Fig. with text S1B). This is because the change in average cell number is not only due to cell division, but also due to cells moving in and out of the observation window. This means that absolute cell division and elongation rates cannot be calculated reliably. However, in some cases, it can still be possible to quantify and assess differences in cell division and cell elongation rates between treatments (see below).

For this study, the measurements did not contain the complete petiole tissue (Fig. 4A,B; every 200 µm class is effectively a separate observation window). Thus, as explained above, we cannot straightforwardly calculate and compare cell elongation and division between the different treatments because the observed changes in cell lengths are due to a combination of actual cell elongation, cell division and cells “moving” in and out of the observation window. Nevertheless, assessing the cell length profile and the tissue characteristics can help to solve these problems. Given that cell size increases towards the distal part of the petiole, it is reasonable to assume that cells move into the observation window at its proximal (near the meristem) border and out at the distal (away from the meristem) border. Furthermore, we can conclude that this process decreases cell size per observation window (smaller cells move into the observation window and larger cells move out of it). Finally, the rate of cells moving in and out of the observation window is determined by the cell elongation proximal of the observation window. From this we can conclude that an increase in observed cell elongation (between two different treatments) can be due to (a combination of) 1) an increase in actual cell elongation, 2) a decrease in cell division, or 3) a decrease in cell elongation proximal of the observation window. After ethylene treatment, we can observe enhanced cell elongation in the most proximal part of the petiole (Fig. 4A,B in the main text), so the last possibility can be discarded. That leaves a combination of decreased cell division and increased cell elongation. The relative contribution of those two factors cannot be quantified using this data alone. We can thus (only) conclude that ethylene treatment increases cell elongation rate relative to cell division rate and that this effect is less strong when *CYCLINA2;1* is constitutively expressed or knocked-out. However, using extra data, namely the shape of the

petiole, we can further analyze cell division and elongation during ethylene treatment using the analysis described in this paper. This analysis yields the abaxial and adaxial cell division rates relative to each other.

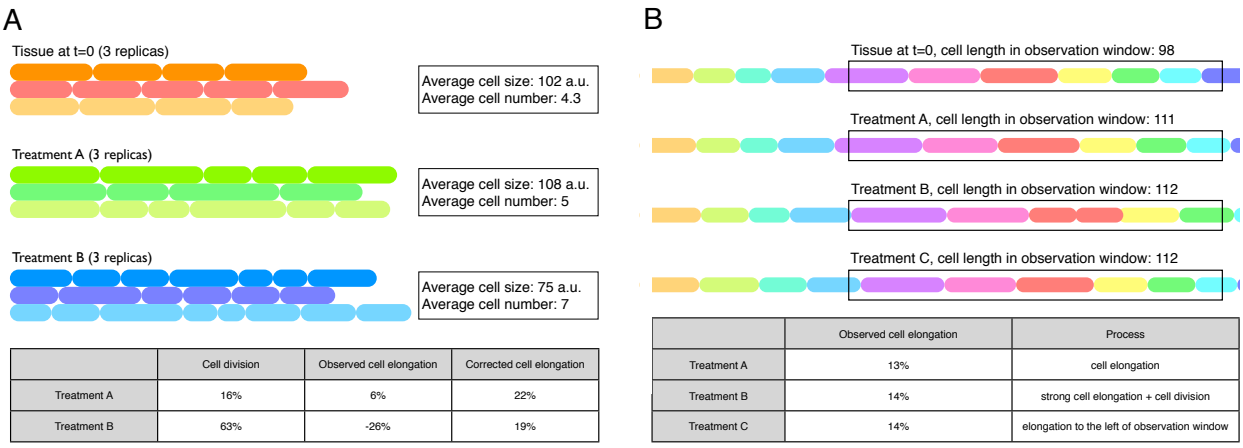

	Cell division	Observed cell elongation	Corrected cell elongation
Treatment A	16%	6%	22%
Treatment B	63%	-26%	19%

	Observed cell elongation	Process
Treatment A	13%	cell elongation
Treatment B	14%	strong cell elongation + cell division
Treatment C	14%	elongation to the left of observation window

Figure with text S1. (A) When analyzing cell elongation and division, it is important to realize that cell divisions reduces cell size, thus observed changes in cell size can not be attributed to cell elongation alone. When cell division rates are known, observed cell elongation can be corrected to obtain actual cell elongation. (B) When the observation window does not cover the whole tissue, it is not straightforward to obtain cell elongation and cell division rates, as a combination of different effects can lead to the same observed cell elongation.

Text S2. Deriving the number of cells from petiole shape and cell lengths

The number of cells along the adaxial and abaxial side of a petiole, n_s and m_s, can be derived from the equations describing petiole shape f(x), and adaxial and abaxial cell length g(x), h(x) (eq. 1-3), where all parameters are fitted to match the experimental measurements. To obtain spatial resolution, the petiole is divided into 50 sections, s, of equal arc length. The absolute coordinates of the endpoint of each section, x_s and y_s, are transformed to x'_s and y'_s, which are the coordinates relative relative to the starting point of each section (eq. 4 & 5) and then rotated to x''_s and y''_s, using the derivative of the function describing the petiole angle, ϕ_s, at the x-coordinate of the end point of the previous section x_{s-1} (where $x_0 = 0$) (eq. 6-8). These transformed coordinates can be used to calculate the radius r_s (eq. 9) and arc length θ_s (eq. 10) of the arc describing the section. Together with the thickness of the petiole, d, these can be used to calculate the length along the adaxial and abaxial side of the section, i_s and j_s, (eq. 11 & 12). Finally, the adaxial and abaxial number of cells, n_s and m_s, is given by the adaxial and abaxial section length divided by the average cell length over the section (eq. 13 & 14).

$$f(x) = ax^2 + bx \tag{1}$$

$$g(x) = a - \frac{b}{1 + \frac{x^2}{c^2}} \tag{2}$$

$$h(x) = a - \frac{b}{1 + \frac{x^2}{c^2}} \tag{3}$$

$$x'_s = x_s - \sum_{t=1}^{s-1} x_t \tag{4}$$

$$y'_s = y_s - \sum_{t=1}^{s-1} y_t \tag{5}$$

$$\phi_s = f(x_{s-1}) \tag{6}$$

$$x''_s = \cos(\phi_s)x'_s + \sin(\phi_s)y'_s \tag{7}$$

$$y''_s = -\sin(\phi_s)x'_s + \cos(\phi_s)y'_s \tag{8}$$

$$r_s = \frac{x''^2_s}{(2 * y''_s)} + \frac{y''_s}{2} \tag{9}$$

$$\theta_s = \arctan(\frac{x''_s}{r_s - y''_s}) \tag{10}$$

$$i_s = (r_s - \frac{d}{2})\theta_s \tag{11}$$

$$j_s = (r_s + \frac{d}{2})\theta_s \tag{12}$$

$$n_s = \frac{i_s - i_{s-1}}{\int_{x=i_{s-1}}^{x=i_s} g(x)} \tag{13}$$

$$m_s = \frac{j_s - j_{s-1}}{\int_{x=j_{s-1}}^{x=j_s} g(x)} \tag{14}$$

Text S3. Profiling of cell proliferation along the petiole

Differential cell proliferation, Δ, within each section, s, (adaxial minus abaxial), can be calculated using the number of cells along the adaxial and abaxial side of the petiole, n_s and m_s. These are derived from the data from the control treatment, the function describing petiole shape, f(x), (eq. 1), and the functions describing the adaxial and abaxial cell length, g(x) and h(x), (eq. 2 & 3), where all parameters are fitted to match the measurements. The adaxial and abaxial section length, i_s and j_s, are obtained by solving equation 4 & 5 for x, where d_s and e_s are adaxial and abaxial cell proliferation rates, which are determined iteratively by minimizing the error in the predicted petiole shape, i.e. eq. 15. The adaxial and abaxial section lengths are used to compute the arc, with radius r_s and arclength θ_s, describing each section (eq. 6 & 7). This arc is used to calculate the relative, rotated, coordinates, x''_s and y''_s, for each section (eq. 8 & 9). This is followed by a back rotation to x'_s and y'_s, according to the angle, ϕ_s, of the function describing the petiole shape at the absolute x-coordinate, x_{s-1} (where $x_0 = 0$), of the endpoint of the previous section (eq. 10-12). Finally the absolute coordinates, x_s and y_s of the section are calculated, taking into account the x-coordinates of the endpoint of the previous sections (eq. 13) and the y-coordinate of the function describing the petiole shape at the x-coordinate of the endpoint of the previous section (eq. 14). Δ_{shape}, the difference between the reconstructed petiole shape and the observed petiole shape (eq. 15) is numerically minimised by introducing and adjusting adaxial or abaxial cell proliferation, d_s and e_s, (where both d_s and e_s are ≥ 1). Because we do not have detailed information on precise localization of petiole elongation, the cell proliferation rates within each section are represented as the difference between adaxial and abaxial cell proliferation, Δ_s, (eq. 16). This is less sensitive for absolute difference in petiole elongation between sections.

$$f(x) = ax^2 + bx \tag{1}$$

$$g(x) = a - \frac{b}{1 + \frac{x^2}{c^2}} \tag{2}$$

$$h(x) = a - \frac{b}{1 + \frac{x^2}{c^2}} \tag{3}$$

$$\frac{i_s - i_{s-1}}{\int_{x=i_{s-1}}^{x=i_s} g(x)} = n_s * d_s \tag{4}$$

$$\frac{j_s - j_{s-1}}{\int_{x=j_{s-1}}^{x=j_s} h(x)} = m_s * e_s \tag{5}$$

$$r_s = \frac{d(i_s + j_s)}{2(j_s - i_s)} \tag{6}$$

$$\theta_s = \frac{j_s - i_s}{d} \tag{7}$$

$$x_s = r_s \sin(\theta_s) \tag{8}$$

$$y_s = r_s - r_s \cos(\theta_s) \tag{9}$$

$$\phi_s = f'(x_{s-1}) \tag{10}$$

$$x'_s = \cos(\phi_s)x_s - \sin(\phi_s)y_s \tag{11}$$

$$y'_s = \sin(\phi_s)x_s + \cos(\phi_s)y_s \tag{12}$$

$$x''_s = \sum_{t=1}^{s} x'_t \tag{13}$$

$$y''_s = \sum_{t=1}^{s} y'_t \tag{14}$$

$$\Delta_{\text{shape}} = (y_s - f(x_s))^2 \tag{15}$$

$$\Delta_s = d_s - e_s \tag{16}$$

Text S4. Influence of cell division on tissue growth

The size of any given tissue is determined by both the size and the number of cells it contains. From this, it follows that tissue growth can be achieved by increasing cell size or increasing cell numbers. However, while increasing cell size directly increases tissue size, an increase in cell number (i.e. cell division without elongation) decreases individual cell size proportionally and thus does not lead to a direct effect on tissue size. However, cell division can influence the growth rate of a tissue indirectly, both positively and negatively, which we here discuss using two examples: linear cell elongation and exponential cell elongation. When cell elongation is linear, it is independent of cell size (Fig. with text S4A), with each cell having an equal contribution to tissue growth. In that case increasing the number of cells proportionally increases the growth rate and hence cell divisions cause an increase in the growth rate of the tissue. In contrast, when the cell elongation is exponential, it is proportional to the cell size (Fig. with text S4B). As a result, larger cells will contribute more to the tissue growth than smaller cells. Because cell division decreases cell size, it proportionally decreases the growth of each individual cell and therefore a tissue consisting of 10 cells of arbitrary length 100 will grow as fast as a tissue consisting of 20 cells of length 50. In short, in this case cell division has no effect whatsoever on tissue growth. The characteristics of the relationship between cell size and cell elongation are not well established (see an in-depth discussion regarding animal cells in Tzur et al, (2009)), but it is reasonable to assume that cell elongation is neither fully dependent nor fully independent of cell size. It can therefore be concluded that cell division in general has a positive indirect effect on tissue growth.

There are additional effects of cell division which can influence the growth rate of a tissue. If we assume that cells have a maximum size, then reducing cell size through cell divisions will allow the tissue to reach a larger final size, if the daughter cells subsequently expand to their maximal size (Fig. with text S4C), even when cells elongate exponentially. It is also possible that during the M-phase of mitosis the rate of cell expansion is reduced, which means that the positive effect of cell division might only be observed on longer timescales, while at shorter timescales tissue growth might decrease due to cell division (Fig. with text S4D).

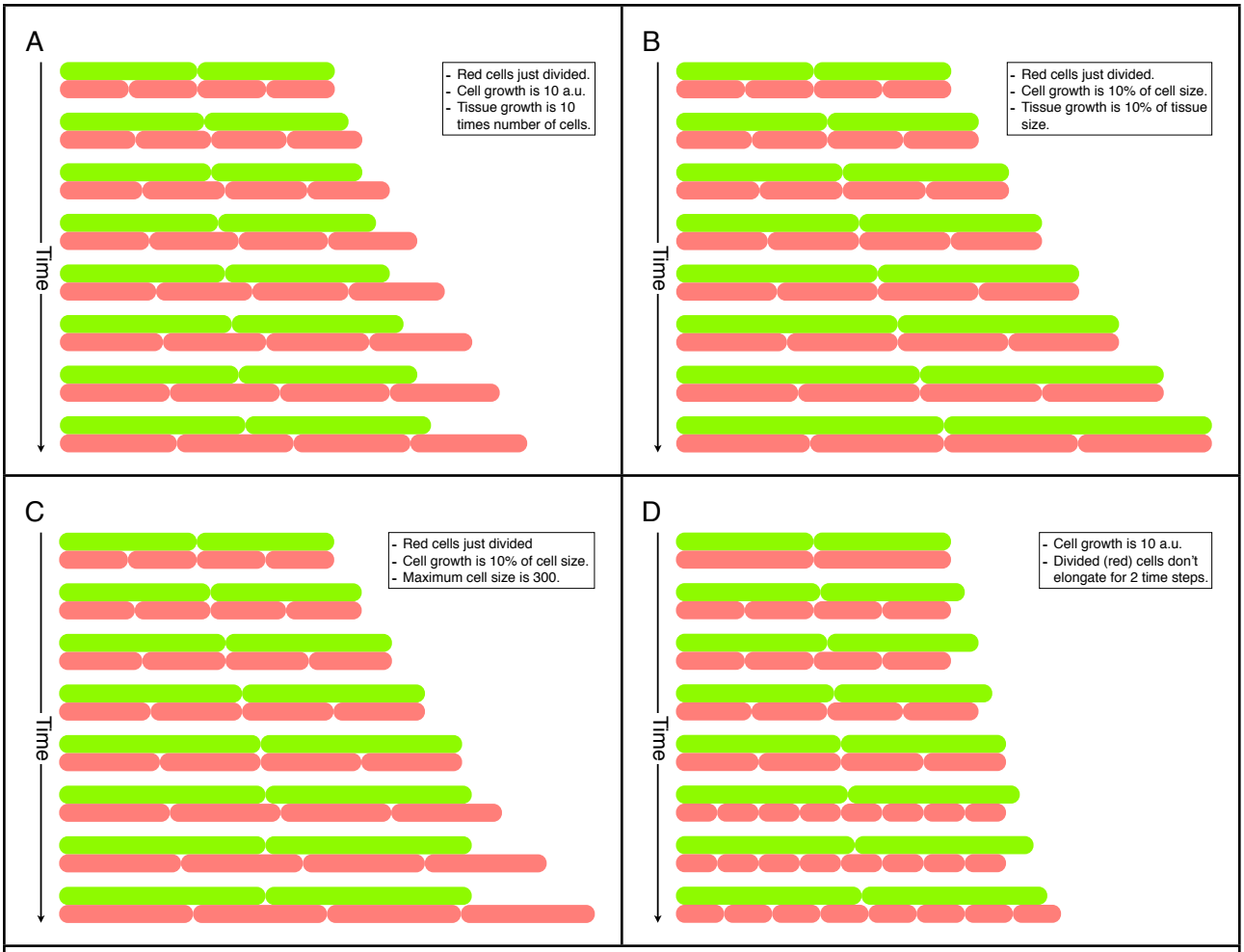

Figure with text S4. A, When cells expand linearly, tissue growth is proportional to the number of cells. Therefore, cell proliferation will lead to increased tissue growth. B, When cells expand exponentially (relative to their length), tissue growth is proportional to tissue size. In this case cell proliferation does not influence tissue growth. C, When cells have a maximum cell length, cell proliferation can increase tissue growth, even if cell expansion is exponential. D, When cells grow less during cell division, a positive effect on tissue growth may only be observed at longer timescales.

Text S5. Additional information for the *in silico* model of the petiole

The relation between cell length (l_{cell}) and cell elongation (δ) is defined in equations 1-4 for linear, exponential, logistic and logarithmic growth respectively, where the 'ρ' parameter indicates growth rate and 'maxlength' indicates maximum cell length for logistic growth. Fig. 1 with text S5, visualizes this relation. The growth rate for the different types of cell growth is synchronized for a cell length of 60 µm. For logistic growth, maximal growth is at a cell length of 124 µm, maximum cell length is 240 µm.

$$\delta(l_{\text{cell}}) = \rho_{\text{linear}} \quad (1)$$

$$\delta(l_{\text{cell}}) = \rho_{\text{exponential}} l_{\text{cell}} \quad (2)$$

$$\delta(l_{\text{cell}}) = \rho_{\text{logistic}} l_{\text{cell}} \left(1 - \frac{l_{\text{cell}}}{\text{maxlength}}\right) \quad (3)$$

$$\delta(l_{\text{cell}}) = \frac{\rho_{\text{logarithmic}}}{l_{\text{cell}}} \quad (4)$$

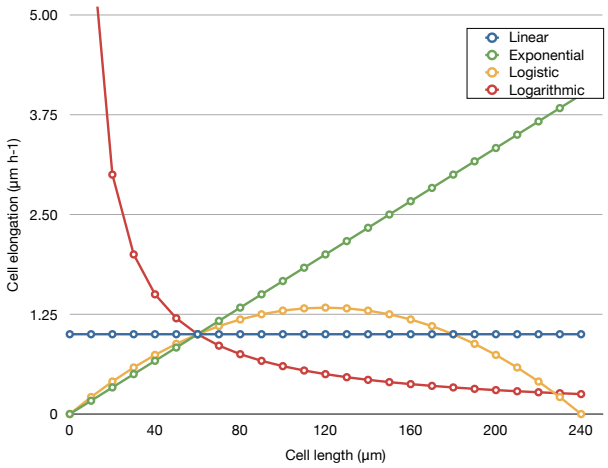

Figure 1 with text S5. Relation between cell length and cell elongation for linear, exponential, logistic and logarithmic growth.

Once cells have reached a threshold cell size, they have an hourly probability to divide. While this minimal cell size has been kept the same for all cells in all simulations, the division probability depends on background (wild-type, *35S::CYCA2;1* or *cyca2;1*), ethylene treatment and whether the cell is located at the adaxial or abaxial side of the petiole, as described in the main text, and with rates indicated in Table S4. In short, the division rate in the *35S::CYCA2;1* background is constitutively high, independent of treatment or cell positioning. In contrast, in the *cyca2;1* background the division rate is constitutively low. Lastly, the wild-type presents an intermediate division rate, which is decreased abaxially under ethylene treatment.

For results shown in Fig. 5B,C in the main text, petiole curvature is used as a proxy for hyponastic growth. The length of the adaxial ($l_{adaxial}$) and abaxial ($l_{abaxial}$) cell rows are used to compute the radius (r) and subsequently the curvature (c) of the petiole (eq. 5 & 6), as is visualized in Fig. 2 with text S5.

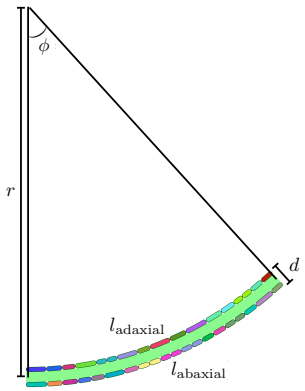

Figure 2 with text S5. Deriving petiole curvature from adaxial and abaxial cell row length.

$$r = \frac{d\,(l_{\text{adaxial}} + l_{\text{abaxial}})}{2\,(l_{\text{abaxial}} - l_{\text{adaxial}})} \quad (5)$$

$$c = \frac{1}{r} \quad (6)$$

$$\phi = \frac{l_{\text{abaxial}} - l_{\text{adaxial}}}{d} \quad (7)$$

In the simulations of hyponastic growth in wild-type, *35S::CYCA2;1* and *cyca2;1* background (results of which are shown in Fig. 5D in the main text), the petioles consists of a proximal (initially 3mm long) and a distal (7mm) part of the petiole. The dynamics of the proximal part are obtained using the *in silico* model, which means that the cells in this part elongate and divide. The cells in the distal part of the petiole are assumed to have reached an equilibrium state and do not elongate or divide. Note that for simplicity cells do not move from the proximal part to the distal part of the petiole during the course of the simulation. The orientation of the distal part of the petiole was obtained by assuming a straight continuation of the modelled, proximal part of the petiole as shown in Fig. 3 with text S5: The angle (ϕ) of the modeled petiole (eq. 7) is equal to the orientation of the extrapolated part of the petiole. From the most distal point of the modeled part of the petiole (($p_{x,y}$); eq. 8 & 9) the most distal point ($q_{x,y}$) of the extrapolated part of the petiole was calculated (eq. 10 & 11), where $l_{extrapolated}$ is 7mm. The petiole angle (α) was measured as the angle between the x-axis and a line from the origin to point $q_{x,y}$ (eq. 12). This point resembles the point that is also used to measure hyponastic growth experimentally in real plants throughout this work. Differential growth (δ) was defined as the change in petiole angle after ethylene treatment minus the change in angle after control treatment and thus resembles the pair-wise subtraction of data (Benschop et al., 2007) that we also used to calculate hyponastic growth in real plants (eq. 13). Fig. 3 with text S5 also shows how to interpret the graphical representation of simulation results (fig 5E-G).

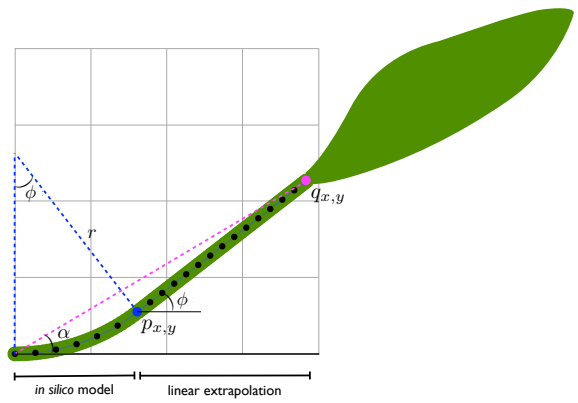

Figure 3 with text S5. Results shown in Fig. 5E-G are to be interpreted as a side-on view of the petiole.

$$p_x = r \sin(\phi) \tag{8}$$

$$p_y = r - r \cos(\phi) \tag{9}$$

$$q_x = p_x + l_{\text{extrapolated}} \cos(\phi) \tag{10}$$

$$q_y = p_y + l_{\text{extrapolated}} \sin(\phi) \tag{11}$$

$$\alpha = \arctan(q_y / q_x) \tag{12}$$

$$\delta = (\alpha_{\text{ethylene}} - \alpha_{\text{t=0}}) - (\alpha_{\text{control}} - \alpha_{\text{t=0}}) \tag{13}$$

Table S1. Initial petiole angles at t=0 h (in degrees ± SEM), of selected *A2-type CYCLIN*-related mutants described in this work.

Col wild-type	22.36 ± 1.38
EHY-D	20.47 ± 1.41
cyca2;1-1	22.01 ± 1.01
cyca2;1-2	16.95 ± 0.79
35S::CYCA2;1 Hmz A	19.07 ± 1.19
35S::CYCA2;1 Hmz B	21.21 ± 0.96
35S::CYCA2;1 HMZ C	23.62 ± 1.73
35S::CYCA2;1 HMZ D	20.41 ± 1.47
ilp1-2	22.95 ± 1.62
ILP1-D	24.01 ± 0.76

Table S2. Primers used for Real-time qRT-PCR. Forward (F) and Reverse (R) gene specific primers, with AGI-code used for Real-time qRT-PCR

AGI-code			
At5g25350	F	CTTTCACGGTGTCCTGGAAT	
	R	GTGGGCAGCTCCTGATAGAG	
At5g25360	F	AAGCCAAGCGTATCAGAGGA	
	R	CAGAGGTTCAATCCGTGGTT	
At5g25370	F	CCGTTATGGCCTGAAGGTAA	
	R	TTCCGGAGGCAAGTATTCAC	
At5g25380	F	ATCAGTTCCCACCACCAAAA	
	R	CCGCGAAATAGTTGGCTAAG	
AT5g25390	F	GACGTGGGAAAAGCAGAGAG	
	R	GACACCTCGGAACTTCTTCG	
AT5g25400	F	CCTTGGATTGTCGTGGAGTT	
	R	CAGAGGTTTTCCCAACCAAA	
At5g25410	F	TGGAGACCCAAAGGAATCAG	
	R	TTGGCAAATGTCAAACTCCA	
At5g25415	F	CATGAACCAGAGACCAGCAA	
	R	GAAGGATCTGAGAGGCAACG	
At5g25420	F	CTGGTTTCAACGGCACTTTT	
	R	GAAATTGAATGGACCGTGCT	
At5g25430	F	CCTATGGCCGGGATATTTTT	
	R	CCGCGTCGTAGAATTCATCT	
CYCA2;1	F	AGCGTGTTGCTAGACCGAGT	
	R	GATTTTTCGCCATCCACATC	
CYCA2;2	F	CGACCAAACTGACCATCCTT	
	R	GCTTTGCCACGCTCTTAAAC	
CYCA1;1	F	GGCTAAGAAGCGACCTGATG	
	R	TACAAGCCACACCAAGCAAC	
CYCA2;3	F	CTCTATGCCCCTGAAATCCA	Yoshizumi *et al.,* 2006
	R	TTTCCATGGAGGAACCAGTC	Yoshizumi *et al.,* 2006
CYCA2;4	F	CAAAGCCTCCGATCTCAAAG	Yoshizumi *et al.,* 2006
	R	CTTGTCCGGTAGCTCTCCAG	Yoshizumi *et al.,* 2006
CYCD3;1	F	GCCACCGTCTCCTCCTCTCTGTAAT	Richard *et al*., 2001
	R	GCCCATGGCAGATGCAAAATCGGCT	Richard *et al*., 2001
CYCB1;1	F	CGAGACGCCCCCACTACTTAGACTT	Richard *et al*., 2001
	R	CGGGTTTAGCTCGAATCGGACATGC	Richard *et al*., 2001
Histone H4	F	CCAAGCCTGCGATCCGAAGATTGGC	Mariconti *et al.,* 2002
	R	CGCTACCGCAAACTGAACGCCAAACCC	Mariconti *et al.,* 2002
ILP1	F	AGCTTGCCAAGAAGGCATTG	Yoshizumi *et al.,* 2006
	R	TCATCAACGACGCAGTCAGA	Yoshizumi *et al.,* 2006

Supplemental references

1. **Benschop JJ, Millenaar FF, Smeets ME, Van Zanten M, Voesenek LACJ, Peeters AJM** (2007) Abscisic acid antagonizes ethylene-induced hyponastic growth in Arabidopsis. Plant Physiol **143**: 1013-1023
2. **Czechowski T, Bari RP, Stitt M, Scheible WR, Udvardi MK** (2004) Real-time RT-PCR profiling of over 1400 Arabidopsis transcription factors: Unprecedented sensitivity reveals novel root- and shoot-specific genes. Plant J **38**: 366-379
3. **Liu YG, Mitsukawa N, Oosumi T, Whittier RF** (1995) Efficient isolation and mapping of *Arabidopsis-thaliana* T-DNA insert junctions by Thermal Asymmetric Interlaced PCR. Plant J **8**: 457-463
4. **Livak KJ, Schmittgen TD** (2001) Analysis of relative gene expression data using real-time quantitative PCR and the 2(-delta delta C(T)) method. Methods **25**: 402-408
5. **Mariconti L, Pellegrini B, Cantoni R, Stevens R, Bergounioux C, Cella R, Albani D** (2002) The E2F family of transcription factors from *Arabidopsis thaliana* - novel and conserved components of the retinoblastoma/E2F pathway in plants. J Biol Chem **277**: 9911-9919
6. **Millenaar FF, Okyere J, May ST, Van Zanten, M, Voesenek LACJ, Peeters AJM** (2006) How to decide? Different methods of calculating gene expression from short oligonucleotide array data will give different results. BMC Bioinformatics **15**: 137
7. **Polko JK, Van Zanten M, Van Rooij JA, Marée AFM, Voesenek LACJ, Peeters AJM, Pierik R** (2012a) Ethylene-induced differential petiole growth in *Arabidopsis thaliana* involves local microtubule reorientation and cell expansion. New Phytol **193**: 339-348
8. **Richard C, Granier C, Inze D, De Veylder L** (2001) Analysis of cell division parameters and cell cycle gene expression during the cultivation of *Arabidopsis thaliana* cell suspensions. J Exp Bot **52**: 1625-1633
9. **Tzur A, Kafri R, LeBleu VS, Lahav G, Kirschner MW** (2009) Cell growth and size homeostasis in proliferating animal cells. Science **325**: 167-171
10. **Weiste C, Iven T, Fischer U, Onate-Sanchez L, Droege-Laser W** (2007) In planta ORFeome analysis by large-scale over-expression of GATEWAY (R)-compatible cDNA clones: Screening of ERF transcription factors involved in abiotic stress defense. Plant J **52**: 382-390

11. **Yoshizumi T, Tsumoto Y, Takiguchi T, Nagata N, Yamamoto YY, Kawashima M, Ichikawa T, Nakazawa M, Yamamoto N, Matsui M** (2006) Increased level of polyploidy1, a conserved repressor of CYCLINA2 transcription, controls endoreduplication in Arabidopsis. Plant Cell **18**: 2452-2468

Table S3. Parameters used to profile cell proliferation rates.

						Petiole shape		Cell length - adaxial (µm)			Cell length - adaxial (µm)		
						$f(x) = ax^2 + bx$		$g(x) = a - \frac{b}{1 + \frac{x^2}{c^2}}$					
		Length	Thickness	Initial angle	Final angle	a	b	a	b	c	a	b	c
Col-0	t=0	10000 µm	700 µm	15.7°	12.0°	-6.5 * 10^{-6}	0.27	201.3	117.6	870.3	233.3	187.8	694.0
	Control	10000 µm	700 µm	15.7°	8.2°	-1.2 * 10^{-5}	0.27	201.3	117.6	870.3	233.3	174.4	598.4
	Ethylene	10000 µm	700 µm	15.7°	22.7°	1.1 * 10^{-6}	0.27	201.3	117.6	870.3	233.3	167.1	439.7
35::CYCA2;1	t=0	10000 µm	700 µm	15.7°	21.2°	9.7 * 10^{-6}	0.27	229.6	193.5	915.4	194.3	156.7	435.1
	Control	10000 µm	700 µm	15.7°	14.2°	-2.5 * 10^{-6}	0.27	229.6	193.5	915.4	194.3	164.0	300.1
	Ethylene	10000 µm	700 µm	15.7°	40.3°	4.4 * 10^{-5}	0.27	229.6	193.5	915.4	194.3	176.2	241.3

Table S4. Parameters used in the *in silico* model.

	cell growth conditions	background	treatment	min cell length for division	cell growth arrest after division	initial population*		initial length***		adaxial cell row		abaxial cell row	
						cell growth**	chance of division	adaxial	abaxial	cell growth**	chance of division	cell growth**	chance of division
figure 5b	indicated in figure			60 µm	no arrest	1 µm h^{-1}	5%	10000 µm	10000 µm	1 µm h^{-1}	5%	1.5 µm h^{-1}	indicated in figure
figure 5c	linear			60 µm	indicated in figure	1 µm h^{-1}	5%	10000 µm	10000 µm	1 µm h^{-1}	5%	1.5 µm h^{-1}	indicated in figure
figure 5d	linear	wild-type	control	60 µm	1 hour	3 µm h^{-1}	10%	2850 µm	3150 µm	3.23 µm h^{-1}	10%	2.75 µm h^{-1}	10%
			ethylene	60 µm	1 hour	3 µm h^{-1}	10%	2850 µm	3150 µm	3.23 µm h^{-1}	10%	3.41 µm h^{-1}	2.5%
		35S::CYCA2;1	control	60 µm	1 hour	3 µm h^{-1}	10%	2850 µm	3150 µm	3.23 µm h^{-1}	20%	2.75 µm h^{-1}	20%
			ethylene	60 µm	1 hour	3 µm h^{-1}	10%	2850 µm	3150 µm	3.23 µm h^{-1}	20%	3.41 µm h^{-1}	20%
		cyca2;1	control	60 µm	1 hour	3 µm h^{-1}	10%	2850 µm	3150 µm	3.23 µm h^{-1}	2%	2.75 µm h^{-1}	2%
			ethylene	60 µm	1 hour	3 µm h^{-1}	10%	2850 µm	3150 µm	3.23 µm h^{-1}	2%	3.41 µm h^{-1}	2%
	exponential	wild-type	control	60 µm	1 hour	3 µm h^{-1}	10%	2850 µm	3150 µm	2.37 µm h^{-1}	10%	2.07 µm h^{-1}	10%
			ethylene	60 µm	1 hour	3 µm h^{-1}	10%	2850 µm	3150 µm	2.37 µm h^{-1}	10%	2.35 µm h^{-1}	2.5%
		35S::CYCA2;1	control	60 µm	1 hour	3 µm h^{-1}	10%	2850 µm	3150 µm	2.37 µm h^{-1}	20%	2.07 µm h^{-1}	20%
			ethylene	60 µm	1 hour	3 µm h^{-1}	10%	2850 µm	3150 µm	2.37 µm h^{-1}	20%	2.35 µm h^{-1}	20%
		cyca2;1	control	60 µm	1 hour	3 µm h^{-1}	10%	2850 µm	3150 µm	2.37 µm h^{-1}	2%	2.07 µm h^{-1}	2%
			ethylene	60 µm	1 hour	3 µm h^{-1}	10%	2850 µm	3150 µm	2.37 µm h^{-1}	2%	2.35 µm h^{-1}	2%
	logistic	wild-type	control	60 µm	1 hour	3 µm h^{-1}	10%	2850 µm	3150 µm	2.80 µm h^{-1}	10%	2.43 µm h^{-1}	10%
			ethylene	60 µm	1 hour	3 µm h^{-1}	10%	2850 µm	3150 µm	2.80 µm h^{-1}	10%	2.92 µm h^{-1}	2.5%
		35S::CYCA2;1	control	60 µm	1 hour	3 µm h^{-1}	10%	2850 µm	3150 µm	2.80 µm h^{-1}	20%	2.43 µm h^{-1}	20%
			ethylene	60 µm	1 hour	3 µm h^{-1}	10%	2850 µm	3150 µm	2.80 µm h^{-1}	20%	2.92 µm h^{-1}	20%
		cyca2;1	control	60 µm	1 hour	3 µm h^{-1}	10%	2850 µm	3150 µm	2.80 µm h^{-1}	2%	2.43 µm h^{-1}	2%
			ethylene	60 µm	1 hour	3 µm h^{-1}	10%	2850 µm	3150 µm	2.80 µm h^{-1}	2%	2.92 µm h^{-1}	2%
	logarithmic	wild-type	control	60 µm	1 hour	3 µm h^{-1}	10%	2850 µm	3150 µm	4.23 µm h^{-1}	10%	3.54 µm h^{-1}	10%
			ethylene	60 µm	1 hour	3 µm h^{-1}	10%	2850 µm	3150 µm	4.23 µm h^{-1}	10%	4.71 µm h^{-1}	2.5%
		35S::CYCA2;1	control	60 µm	1 hour	3 µm h^{-1}	10%	2850 µm	3150 µm	4.23 µm h^{-1}	20%	3.54 µm h^{-1}	20%
			ethylene	60 µm	1 hour	3 µm h^{-1}	10%	2850 µm	3150 µm	4.23 µm h^{-1}	20%	4.71 µm h^{-1}	20%
		cyca2;1	control	60 µm	1 hour	3 µm h^{-1}	10%	2850 µm	3150 µm	4.23 µm h^{-1}	2%	3.54 µm h^{-1}	2%
			ethylene	60 µm	1 hour	3 µm h^{-1}	10%	2850 µm	3150 µm	4.23 µm h^{-1}	2%	4.71 µm h^{-1}	2%

*for initial population linear growth conditions are used in all cases.

**value corresponds to the result of eq. 1-4 in appendix S5 for a cell length (l_{cell}) of 60 µm.

***the values given for figure 5d are for the proximal part of the petiole, see appendix S5.